J. Fluid Mech. (1995), *vol.* 296, *pp.* 127–157

Energetics of grid turbulence in a stably stratified fluid

By HSIEN-TA LIU
QUEST Integrated, Inc., Kent, WA 98032, USA

(Received 6 May 1992 and in revised form 7 February 1995)

A biplane grid with a mesh spacing of 10.8 cm was towed horizontally in a towing tank to generate turbulence in a non-stratified fluid and in stratified fluids with different constant density gradients. Turbulence velocity components and density fluctuations were measured using an array of cross-film and conductivity probes. Based on the mesh size of the grid, the nominal values of the (internal) Froude numbers were ∞, 80 and 40, and the corresponding Reynolds number was 4.3×10^4. The decay rates of the (turbulence) kinetic, potential and total energies and the dissipation rates of the kinetic and potential energies were calculated from the experimental data. For each of these quantities, the decay may be represented as a function of the downstream distance raised to a given power. The kinetic energy and its dissipation rate are lower for the stratified cases than for the non-stratified case but are almost compensated for by the corresponding potential energy and its dissipation rate. Our results are consistent with those of direct numerical simulations and agree reasonably well with those obtained in stratified wind and water tunnels. However, the results differ from laboratory results obtained using an optical method to measure the turbulent motion of tracer particles in the wake of a vertically towed grid; these latter results show an abrupt reduction in the decay rate of the turbulence kinetic energy after one Brunt–Väisälä period. A similar trend is also observed in results obtained in facilities with fairly high background turbulence or internal waves. This discrepancy is discussed and an explanation is presented. Furthermore, it is demonstrated that strongly stratified thin sheets with density gradients larger than that of the undisturbed fluid may be generated by local but incomplete mixing. The persistence of such thin sheets is proportional to the Schmidt number (≈ 500) in stratified salt water or the Prandtl number (≈ 0.71) in thermally stratified air.

1. Introduction

Most investigations of grid-generated turbulence reported in the literature have been conducted in non-stratified or homogeneous fluids (e.g. Comte-Bellot & Corrsin 1971). To measure the decay of grid turbulence in a density-stratified fluid, Lin & Veenhuizen (1974) and Dickey & Mellor (1980) (hereafter respectively referred to as L & V and D & M) conducted experiments in horizontal and vertical towing tanks, respectively. These two groups used two entirely different experimental methods, and their results contradict each other. Specifically, D & M's data show an abrupt reduction in the decay rate of the turbulence kinetic energy after one Brunt–Väisälä (B–V) period, whereas L & V's data show that with a relatively strong stratification no abrupt change occurs for up to five B–V periods. According to D & M, the abrupt change signals the transition from a turbulence-dominated regime to an internal-wave-dominated regime.

Other laboratory investigations (Britter *et al.* 1981; Stillinger 1981) have added further controversy to the phenomenon of turbulent flows in a stratified fluid.

It is essential to understand the effects of stratification on turbulence so that a physically consistent turbulence model can be developed for use in numerical simulations of turbulent flows in a stratified fluid. The results of direct numerical simulations of turbulence in a stratified fluid using a spectral method (Riley, Metcalfe & Weissman 1981), which did not require the use of a turbulence model, showed that the decay rate of the turbulence kinetic energy did not have an abrupt transition. Other data on stratified wakes of towed and self-propelled bodies have been reviewed by Lin & Pao (1979). Again, the decay characteristics in such localized wakes show no sign of an abrupt transition for up to about 10 B–V periods (Lin, Pao & Veenhuizen 1974; Lin & Pao 1979). Britter *et al.* (1981) argued that a mean oscillatory motion of the entire water column, which is likely to be generated by the vertically towed grid used by D & M, is a possible source for the slowly decaying fluctuations. Subsequently, Van Atta, Helland & Itsweire (1984) pointed out that the intense generation of internal waves near the grid may lead to this type of behaviour. This was further demonstrated by Itsweire, Helland & Van Atta (1986), who attempted to separate the contribution of the internal-wave motion and the vertical component of the turbulence kinetic energy.

Most recently, Lienhard & Van Atta (1990) and Yoon & Warhaft (1990) conducted experiments in thermally stratified wind tunnels that were designed to prevent the formation of standing internal waves in the test section. The reported wind-tunnel results, however, are limited to small buoyancy times of less than 0.8 B–V period before the stratified turbulent fluid is swept downstream of the test section by the mean flow. The wind-tunnel results do not reach the critical time of one B–V period, at which D & M observed an abrupt reduction in the turbulence kinetic energy.

The present investigation involves a series of experiments conducted in a stratified towing tank. It includes measurements of the instantaneous velocity and density fields in the wake of a biplane grid. The measurements were conducted using a vertical array of cross-film and conductivity probes towed at the same speed as the grid in the horizontal direction. The Reynolds number based on the mesh size is

$$R = UM/\nu \approx 4.3 \times 10^4, \tag{1}$$

where U is the towing speed, M is the mesh spacing of the grid and ν is the kinematic viscosity. This mesh Reynolds number is about the same as that of D & M and L & V but is about a factor of 5 greater than that of the wind-tunnel experiments (e.g. Lienhard & Van Atta 1990). Experiments were conducted for three (internal) Froude numbers defined as

$$F = U/NM \approx \infty, 80 \text{ and } 40. \tag{2}$$

Here, N is the B–V frequency in Hertz, defined as

$$N = \frac{1}{2\pi}\left(\frac{g}{\rho_0}\frac{\mathrm{d}\bar{\rho}}{\mathrm{d}z}\right)^{1/2}, \tag{3}$$

where g is the gravitational acceleration, $\mathrm{d}\bar{\rho}/\mathrm{d}z$ is the ambient (constant) vertical density gradient and ρ_0 is a reference density. By definition, the Froude number is proportional to the ratio of the inertial force to the buoyant force of the stratified flow. For $F \to \infty$, the experiments were conducted in a homogeneous fluid. The results obtained by L & V, who used a single-plane grid in the same facility for $F \approx 20$, are included in our analysis to extend the data to a lower Froude number for comparison. We reanalysed their original data, however, using the analysis procedure developed for

the present data set (§4). Quantitative comparison of these two sets of data is not possible owing to the geometrical differences in the two grids. Qualitative comparison of the data, however, can be made to observe any significant differences in the trend of the turbulence characteristics for Froude numbers below the range considered in the present investigation.

In the present laboratory investigation, new experimental evidence on the characteristics of grid turbulence in a salt-stratified fluid is presented to explain and resolve the above controversy. This paper concentrates on the decay characteristics of the turbulence kinetic and potential energies and the dissipation rates of stratified grid turbulence for Nt up to five B–V periods, significantly beyond those that have been measured in a wind or water tunnel. In §2, a brief literature review of grid turbulence relevant to the present investigation is provided. The experimental facility, instrumentation and experimental procedures are described in §3, and the procedures for data analysis are presented in §4. In §5, we discuss the laboratory results. We then summarize, in §6, the important findings derived from the present investigation. Finally, we present arguments in §7 to account for the discrepancy between our results and those of D & M. To support one of the arguments, we present measurements of the apparent velocity fluctuations of a stationary object in a turbulent stratified fluid.

2. Literature review

A brief review of previous work on grid turbulence in homogeneous and stratified fluids is provided in this section. Most grid-turbulence experiments have been conducted in wind tunnels (e.g. Comte-Bellot & Corrsin 1966; Schedvin, Stegen & Gibson 1974). Only a very few studies have been conducted in either a water flume or towing tank (e.g. Friehe & Schwarz 1970). Laboratory results show that grid turbulence is only approximately isotropic with $\overline{v^2} \approx \overline{w^2} \approx 0.83\overline{u^2}$ for a straight duct (Comte-Bellot & Corrsin 1966), where u, v and w are the longitudinal, transverse and vertical velocity components, respectively. Comte-Bellot & Corrsin (1966) improved grid-turbulence isotropy by using a duct with a small contraction ratio (1.27:1). In general, the components of the turbulence kinetic energy decrease with the downstream distance, x, according to the following power law (see Gad-el-Hak 1972):

$$\frac{\overline{u^2}}{U^2} = a_1\left(\frac{x}{M}\right)^{-n}, \quad \frac{\overline{v^2}}{U^2} = a_2\left(\frac{x}{M}\right)^{-n}, \quad \frac{\overline{w^2}}{U^2} = a_3\left(\frac{x}{M}\right)^{-n} \tag{4}$$

where a_1, a_2 and a_3 are constants, n ranges from 1.0 to 1.6 and U is the free-stream mean wind speed. For most data, the longitudinal component of the turbulence kinetic energy may be represented by

$$\overline{u^2}/U^2 \approx 0.5(x/M)^{-1.3}. \tag{5}$$

Lange (1974) towed a biplane grid of cylindrical bars in a stably stratified towing tank to study the Lagrangian diffusion of scalar quantities, in particular the suppression of diffusion by stratification and the transition of the turbulence into internal waves. L & V conducted experiments to study grid-generated turbulence in a stratified towing tank. To demonstrate the extreme effect of stratification on the turbulence characteristics, they chose the very low Froude number of 20. For this low Froude number, they found that the horizontal elements of a biplane grid are a strong source of internal waves. Thus, the turbulence generated by a biplane grid is highly anisotropic, as can be observed from shadowgraph pictures (Lin & Pao 1979). Consequently, Lin & Pao chose to use a single-plane grid composed of vertical square rods. The components of instantaneous velocity and density in the wake of the grid

were measured with an array of cross-film and conductivity probes, respectively. Their measurements show that the mean squares of the components of velocity fluctuations, as a function of the dimensionless distance downstream of the grid, x/M, generally follow a power law such as that expressed in (5). The vertical turbulent motion decays faster than its horizontal counterpart, indicating an inhibition of vertical motion by stratification. The dissipation rate, from the derivative of the longitudinal component of the velocity, also follows a power law decay. It should be noted that the present author found that noise had not been subtracted from the reported findings by L & V or by Lin & Pao (1979).

Experiments were also conducted by Lin *et al.* (1974) to investigate the turbulence characteristics in the wakes of towed and self-propelled slender bodies (see also Lin & Pao 1979). The decay of the longitudinal component of the turbulence kinetic energy follows a -1.5 power law for $0.1 \leqslant Nt \leqslant 3$. The power index increases slightly for $Nt > 3$, suggesting a smaller dissipation rate. The vertical component of the turbulence kinetic energy decays as $(Nt)^{-2}$ for $0.1 \leqslant Nt \leqslant 8.5$. It is suspected that the significant difference in the decay rate between the horizontal and vertical components is due to internal-wave radiation from the wake, which is not present in the grid experiments. No evidence of a reduction in the decay rate was observed for these components. The turbulence potential energy, which is proportional to the mean square of the density fluctuations, decays as $(Nt)^{-2}$ for $0.7 \leqslant Nt \leqslant 10$. For Froude numbers (based on the maximum body diameter) ranging from 23 to 120, the decay of the maximum value of the turbulence kinetic energy is found to be dependent on the Froude number.

D & M, using an optical method, measured the motion of seeded particles in the wake of a biplane grid towed vertically. The mesh Reynolds number was 4.8×10^4, which is comparable to that of L & V. The components of the velocity fluctuations of small tracer particles, assumed to be equal to those of the fluid, were derived from time-lapse photographs of the seeded flow. Measurements were conducted in a homogeneous fluid and in a stratified fluid with a constant density gradient ($N = 0.06$ Hz). The Froude number for the stratified case was about 312, which is much higher than that in the experiments conducted by L & V. The results of D & M show a dramatic difference in the decay of turbulence kinetic energy between the non-stratified and stratified runs. In particular, the turbulence kinetic energy for the stratified run almost ceases to decay, that is the decay rate reduces abruptly, for dimensionless downstream distances greater than about 300. The abrupt transition occurs equivalently at about one B–V period after passage of the grid. If such an abrupt transition were to be attributed to stratification, as suggested by D & M, one would expect to detect a more pronounced transition for the lower Froude number counterpart.† However, no such transition is observed in the data reported by L & V for up to five B–V periods. No explanation was offered by D & M to account for this discrepancy.

From experiments conducted in the wake of a biplane grid Britter *et al.* (1981) inferred the velocity fluctuations in the stratified cases from the standard deviation of the vertical or lateral plume spread by using the statistical theory of diffusion. Their comparison of velocity fluctuations in a homogeneous fluid and in stratified fluids ($F \approx$ 53 to 3.1) did not show a significant difference in the decay rate of the kinetic energy. Their data do not show an abrupt transition in the decay rate of the kinetic energy, even for the extremely low Froude number case, $F \approx 3.1$. They argue that a mean

† An inconsistency exists in D & M's comparison of their data with those of L & V because D & M measured the B–V frequency in radians per second and L & V used Hertz. As a result, the ratio between the Froude number of the experiments of D & M and that of L & V, reported by D & M to be 2.5, is actually about 16.

oscillatory motion is likely to be generated by the vertically towed grid used by D&M, which could be a possible source for the slowly decaying fluctuations.

Stillinger, Helland & Van Atta (1983) conducted a series of grid-turbulence experiments in a closed-loop density-stratified water channel. Their results show that an abrupt change occurs in the decay rate of the turbulence kinetic energy for the stratified cases, as was reported by D&M. In the stratified water channel, the installation of a turbulence management section consisting of grids and foam was necessary to smooth discrete jumps present in both the density and velocity profiles (Stillinger 1981). As a result, the background turbulence in the free stream was comparatively high, typically 1.5% of the free-stream mean speed in a non-stratified fluid (increasing to about 3.5% without the management section). The background turbulence, which is in effect 'noise' to the grid-generated turbulence, has not been removed from the data reported. In a stratified fluid, the turbulence management section would act as an internal-wave generator, as acknowledged by Stillinger (1981). Therefore, the abrupt change in the decay rate of the turbulence kinetic energy is likely attributable to high background turbulence and/or to internal waves generated by the management section; the former is consistent with the trend demonstrated by Stillinger (1981, p. 52, figure 3–5). Van Atta *et al.* (1984) attributed the relatively low decay rate of the vertical component of the turbulence kinetic energy in Stillinger's data to the intense internal waves generated near the grid. This is subsequently demonstrated by Itsweire *et al.* (1986), who made an attempt to separate the contribution of the internal-wave motion to the vertical component of the turbulence kinetic energy.

In the late 1980s, thermally stratified wind tunnels were developed to study grid turbulence in a stratified fluid (Lienhard & Van Atta 1990; Yoon & Warhaft 1990). There is a fundamental difference between air and water experimentation in that the Prandtl number for air (≈ 0.71) and the Schmidt number for salt water (≈ 500) differ greatly. We anticipate that the dissipation of salinity fluctuations in water will take much longer than the dissipation of temperature fluctuations in air. This difference must be taken into consideration when comparing experimental results measured in air and in salt water. There are advantages and disadvantages in studying stratified turbulence in the two media. For example, the accuracy in scalar and velocity measurements is generally higher in air than in salt water. Wind tunnels may be specially designed to avoid standing internal waves in the test section. On the other hand, the mesh Reynolds numbers are about a factor of 5 lower in wind-tunnel than in salt-water experiments. The Froude numbers achievable in wind tunnels are high compared to those in salt water facilities (particularly towing tanks). Furthermore, available wind-tunnel results are limited to a small buoyancy time of less than 0.8 B–V period before the stratified turbulent fluid is swept downstream of the test section by the mean flow. (For the same reason, the buoyancy time for the results obtained in a salt-stratified water tunnel is considerably shorter than that obtained in a towing tank.) Within the small buoyancy time, there are findings such as the initial build up of the (turbulence) potential energy and the subsequent interexchange in turbulence kinetic energy and potential energy that either do not occur or cannot be accurately measured in the salt-stratified counterpart. In the absence of measurements beyond 0.8 B–V period, however, the wind-tunnel results do not offer direct experimental evidence to resolve the controversy concerning the decay rate of the turbulence kinetic energy at one B–V period and beyond and to demonstrate whether the presence of internal waves is responsible for the reduction in the decay rate, as reported by D&M. The towing tank is most suitable for low Froude number experiments that would allow us to observe the evolution of stratified turbulence up to five or more B–V periods.

A series of direct numerical simulations of homogeneous turbulence in density-stratified fluids was conducted by Riley *et al.* (1981). Using pseudospectral methods, they solved directly the fully nonlinear equations of motion so that closure assumptions were not necessary. The simulations were a direct extension of the work by Orszag & Patterson (1972), who performed direct numerical simulations of homogeneous decaying turbulence. The method of Orszag & Patterson involved the initialization of a statistically homogeneous and isotropic velocity field defined in terms of a vector potential. Then, the stratification was imposed and the velocity field was allowed to evolve according to the governing Navier–Stokes equations. Riley *et al.*'s results show no abrupt transition in the decay of turbulence kinetic energy. They found, however, that stratification introduces wave-like characteristics into the flow fields. This is exemplified by the exchange between kinetic and potential energy. The dissipation of kinetic energy is significantly decreased; however, this is almost entirely compensated for by the dissipation of potential energy. Stratification also inhibits the spectral transfer of kinetic energy, but this also is almost entirely compensated for by the spectral transfer of potential energy.

The Reynolds number in the simulation by Riley *et al.* (1981) was too low to allow direct comparison with experiments. Métais & Herring (1989) performed another series of direct numerical simulations for a higher Reynolds number, comparable to that of Itsweire *et al.* (1986). The Prandtl number accessible numerically was of order unity, however, which is about two orders of magnitude lower than the Schmidt number of the salt-stratified experiments. Reasonable agreement between the computed and experimental results was reported; the oscillatory buoyancy flux is more strongly damped in the latter than in the former – plausibly attributable to the above differences in the Prandtl and Schmidt numbers.

3. Experimental facility and procedure

A description of the laboratory facility has been given by Liu (1992). The facility consists of a towing tank, a filling system, a towing system, two oil-bearing carriages and several traversing mechanisms. A set of instruments, supported by a Data General minicomputer (NOVA 800) and peripherals for on-line data acquisition and analysis, is available for quantitative measurements of a variety of physical variables.

The towing tank measures 18 m long, 1.2 m wide and 0.9 m deep (Liu 1992). A special filling system was designed to provide the homogeneous and stratified fluids. Tap water was used to prepare a homogeneous fluid. The tap water was first heated to room temperature using a Paypack gas-fired water heater and then filtered with a 10-μ Culligan depth filter. To prepare a stratified fluid, the filling was started with fresh water. Then a NaCl solution of increasing density was fed slowly from the bottom through three feeder channels. The density of the NaCl solution was controlled by mixing concentrated brine with fresh water fed from two separate constant-head tanks through a mixing valve. It took 6 h to prepare a stratified tank and at least 3 h for the tank to settle before any measurements could be made. Normally the tank was prepared in the evening, and experiments were conducted in the daytime. A fresh tank was prepared every day for stratified runs and every 2 to 3 days for the non-stratified runs. No more than three runs were conducted each day, and there was a 3-h wait between runs.

The towing system included two sets of towing cables, drive pulleys, drive shafts and motors and controllers. It was designed to tow two oil-bearing carriages independently or simultaneously. The carriages, one for towing the grid and the other for the probe

array, rode on a thin film of oil released from four pads supporting the carriages on two tracks, one round and one flat. The tracks were carefully aligned so that the vertical displacement of the instrumentation carriage was within 2 mm in the 12 m working section. A slotwheel consisting of 16 slots was attached to the drive shaft of each motor, and a light emitter/photosensor set was used to measure the towing speed.

The grid was made of wood having a square cross-section of 1.27 cm × 1.27 cm. It had a mesh size of 10.8 cm and a solidity of 0.2. The grid was mounted on one of the oil-bearing carriages and towed at a nominal speed of 40 cm s^{-1}. A vertical array of cross-film probes (Thermo-Systems, Inc., (TSI) 1248Y-NACL) connected to a TSI anemometer (Model 1053B) was used to measure the three velocity components in the wake of the grid. The elements of the cross-film probes were 0.0025 cm in diameter and 0.025 cm in length. At a speed of 40 cm s^{-1}, the frequency response of the probes in water was estimated to be better than 800 Hz, according to the specifications (available from the TSI catalogue). For the density measurements, single-electrode conductivity probes, together with a 10-channel conductivity gauge manufactured by Flow Research Company (Model 1010), were used. The tip of the conductivity probe was made of a platinum wire 0.13 mm in diameter. The wire was protected by a small glass tube 1.6 mm in diameter, which was drawn down at the probe tip. The tip was coated with a platinum black solution to attain high sensitivity. Calibration of the probe in a two-dimensional buoyant jet showed that the spatial resolution at a speed of 40 cm s^{-1} was better than 1 mm, which is about the Kolmogorov microscale in water (in the range of Reynolds numbers considered here). Each conductivity probe was mounted in close proximity to a hot-film probe. The tip separation was about 1.3 mm centre to centre, which was the minimum separation for avoiding probe interference. This probe configuration was designed to measure the density flux in the stratified fluid. The cross-film and conductivity probe pairs were mounted on a stainless-steel strut (1.3 cm thick and 15 cm wide) with streamlined leading and trailing edges. The strut was mounted on a two-dimensional manual traverse that was part of the carriage. The traverse was used for alignment as well as for calibration of the conductivity probes.

During each experiment, the array of probes was towed at a predetermined distance behind the grid and at the same speed as the grid. For small x/M (< 20), both carriages were mounted on a single towing system; for large x/M (> 20), they were mounted on separate towing systems. The velocity and conductivity data were sampled at 833 Hz (520 Hz for the homogeneous cases), and the signals were low-pass filtered at 400 Hz. For the non-stratified or homogeneous cases, the velocity components were the only quantities to be measured. Immediately before a run, we turned on all the hot-film probes to the RUN position on the anemometers. During a run, the grid was towed ahead of the probe array. Data recording began as soon as the probe array moved into the working section of the tank, and it stopped automatically at the end of the tow. Post calibration of the cross-film probes was made about 15 min after each run. The array of probes was towed at five different speeds to span the anticipated range of flow speeds for the run. We waited at least 2.5 h before conducting the next run. A second-degree polynomial, instead of the King's law, was used to fit the calibration data.

For the stratified runs, additional measurements of the density field were made prior to the tow. First, the density profile was measured with a conductivity probe mounted on a vertical traverse. The probe was calibrated by using five solutions of NaCl with different densities covering the range of densities of the working fluid in the tank. The temperature of the jars was matched to within 0.1 °C of the working fluid. In figure 1, vertical profiles of the reduced density, defined by $\sigma = (\rho - 1) \times 10^3$, where ρ is the fluid density in g cm^{-3}, and the corresponding B–V frequencies are plotted. The density

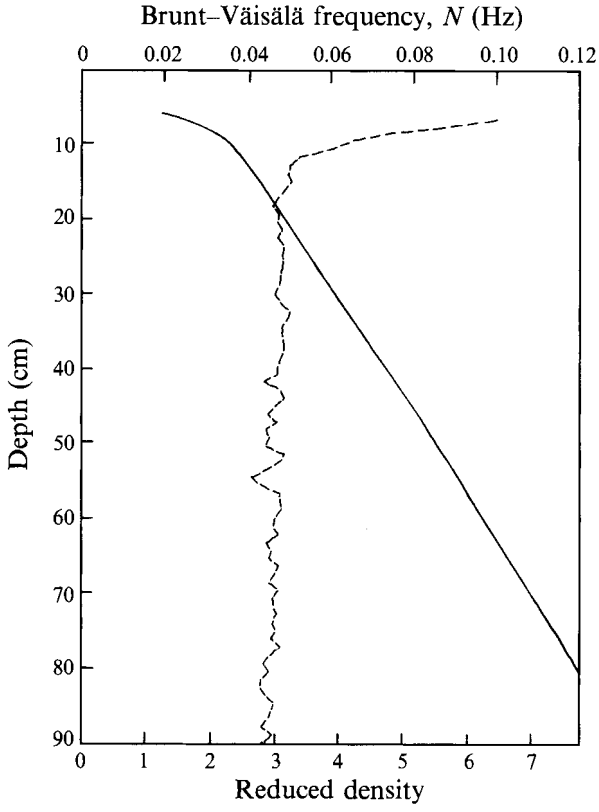

FIGURE 1. Vertical profiles of density stratification (——) and corresponding Brunt–Väisälä frequencies (---).

gradients are reasonably linear, except near the top 10 cm where the density profile is modified significantly due to evaporation at the water surface. As soon as the density profile was measured, the conductivity probes mounted on the probe strut were calibrated against the measured density profile in the tank. To do so, the probes were placed at five vertical positions at predetermined increments. At each position, the voltage outputs of the conductivity probes and the corresponding vertical distance of the position were recorded. The calibration values for the probes were derived from the recorded voltages and the vertical positions, with reference to the vertical density profile just measured. Second-degree polynomials were used to fit the calibration data, although the data appeared to be linear. After completion of the above calibration, we then proceeded to execute the rest of the run using the procedure described above for the non-stratified cases. The only difference was that both hot-film and conductivity probes were used in the stratified cases.

4. Data analysis

In this section, we first define the physical quantities to be derived from the experimental results. We then describe the procedure for data analysis and the expected errors for the experimental results.

4.1. *Physical quantities*

In a homogeneous fluid, the total (turbulence) energy or TE is the total turbulence kinetic energy or TTKE, which is the sum of the three components of the turbulence kinetic energy or TKE:

$$\text{TE} = \text{TTKE} = \tfrac{1}{2}(\overline{u^2}+\overline{v^2}+\overline{w^2}). \tag{6}$$

In a stratified fluid, (turbulence) potential energy or PE is directly generated by passage of the grid and subsequently converted from (and to) turbulence kinetic energy. The potential energy may be expressed in terms of the density fluctuations for a constant-density-gradient fluid (Holliday & McIntyre 1981):

$$\text{PE} = -\frac{1}{2}\frac{g}{\rho_0}\left(\frac{\mathrm{d}\bar{\rho}}{\mathrm{d}z}\right)^{-1}\overline{\rho^2}, \tag{7}$$

where ρ_0 is a reference density and $\mathrm{d}\bar{\rho}/\mathrm{d}z$ is the density gradient. Using the definition of the B–V frequency in §1, we have

$$\text{PE} = \frac{1}{2}\left(\frac{g}{\rho_0 2\pi N}\right)^2\overline{\rho^2}. \tag{8}$$

The total energy is therefore the sum of the total turbulence kinetic energy and the potential energy:

$$\text{TE} = \text{TTKE}+\text{PE}. \tag{9}$$

From the experimental data, we may estimate the kinetic energy dissipation rate according to the formula derived for locally isotropic turbulence (Hinze 1959):

$$\epsilon = 15\nu\overline{(\partial u/\partial x)^2}, \tag{10}$$

or

$$\epsilon = (15\nu/U^2)\overline{(\partial u/\partial t)^2}, \tag{11}$$

using Taylor's hypothesis, where ν is the kinetic viscosity and t is the time. Therefore, we may estimate the dissipation rate from the mean square of the time derivatives of the longitudinal turbulence velocity fluctuations. Another method to estimate the dissipation rate is to use the velocity spectrum, which is by definition

$$\epsilon = 15\nu\int_{k_0}^{k_c} k^2 E_u(k)\,\mathrm{d}k. \tag{12}$$

Here, $E_u(k)$ is the one-dimensional wavenumber spectrum, k is the wavenumber, k_0 is the smallest wavenumber resolved in the spectral computation and k_c is an upper wavenumber cutoff chosen to avoid the noise contamination generally present in the highest-wavenumber portion of the spectrum. The radian wavenumber, k, is related to the frequency f (in Hertz) by $k = 2\pi f/U$. The dissipation rate can then be expressed as

$$\epsilon = \frac{15\nu}{U^2}\int_{f_0}^{f_c}(2\pi f)^2 E_u(f)\,\mathrm{d}f, \tag{13}$$

where f_0 and f_c correspond to k_0 and k_c. In most cases, f_c is between 100 and 200 Hz, but it can be as low as 40 Hz at $x/M \geqslant 200$. A comparison of the dissipation rate that is estimated from the mean square of the longitudinal velocity derivatives (noise subtracted) and the rate from the spectrum agrees to within 10%. The dissipation rate presented in our results (§5) was estimated from the velocity spectrum.

The dissipation of density variance, χ, is defined by

$$\chi = 2D\overline{(\nabla\rho)^2}, \tag{14}$$

where D is the molecular diffusivity of NaCl, which was used to make up the stratified fluid. For isotropic turbulence, χ may be defined in terms of the longitudinal density gradient by

$$\chi = 6D\overline{(\partial\rho/\partial x)^2}. \tag{15}$$

Direct calculation of χ from the one-dimensional density spectrum E_ρ is given by

$$\chi = 6D\int_{f_0}^{\infty}(2\pi f)^2 E_\rho(f)\,\mathrm{d}f. \tag{16}$$

Another method for estimating the dissipation rate of the density variance was developed by Batchelor (1959) under the assumption that a k^{-1} or f^{-1} subrange exists. The theoretically expected form is given by

$$E_\rho(k) = \beta(\nu/\epsilon)^{1/2}\chi_\beta k^{-1}, \tag{17}$$

or

$$E_\rho(f) = \beta(\nu/\epsilon)^{1/2}\chi_\beta f^{-1}, \tag{18}$$

where the constant β was assumed to be 3.0, from the range of values between 2 and 6 as reported by Williams & Paulson (1977). When $fE_\rho(f)$ is plotted versus f, the Batchelor subrange is manifested as a flat region in the spectrum with a cutoff at higher wavenumbers. Then, χ_β can be estimated from the level of the flat region, $E_\rho(f_\beta)f_\beta$, according to (18):

$$\chi_\beta = \beta^{-1}E_\rho(f_\beta)f_\beta(\epsilon/\nu)^{1/2}, \tag{19}$$

where f_β is the frequency range in which the Batchelor subrange is observed. Comparison of the dissipation rates of the density variance, as derived from the two methods discussed above, shows that the value derived from (15) or (16) is consistently much lower than that from (19). In fact, the ratio of the two values estimated from the data measured at $x/M = 27.3$ is approximately 0.01. According to Batchelor (1959), for a large Schmidt number ($D \ll \nu$), the Batchelor subrange extends to a much higher wavenumber, $(k_m)_\rho \approx (\epsilon/\nu D^2)^{1/4}$, than that of the velocity equilibrium range, $(k_m)_u \approx (\epsilon/\nu^3)^{1/4}$. The corresponding spatial resolutions (frequency responses) required are, respectively, 0.01 cm (3900 Hz) and 0.27 cm (146 Hz). Note that the spatial resolution of the conductivity probe, consisting of a 0.13 mm diameter platinum wire, is about 0.1 cm. The attenuation at high frequencies due to insufficient spatial resolution of the conductivity probe contributes to the above discrepancy, because the value of χ heavily weighs the high-frequency components due to the f^2 factor in (16). However, the spatial resolution of the conductivity probe is more than adequate to measure the potential energy, because the spectral density is negligible at wavenumbers higher than that corresponding to the spatial resolution of the conductivity probes

Our results show that the one-dimensional spectra of the density fluctuations demonstrate the existence of an f^{-1} region, except at large x/M for $F < 40$. Therefore, (18) was used to estimate the dissipation rate of the density variance. To derive the dissipation rate of the potential energy, the following equation is used according to (8):

$$\chi_p = (g/(2\pi N\rho_0))^2\chi_\beta. \tag{20}$$

Both dissipation rates are then made dimensionless by multiplying by a common factor of M/U^3; that is,

$$\epsilon^* = \epsilon M/U^3 \tag{21}$$

and

$$\chi_\rho^* = \chi_\rho M/U^3. \tag{22}$$

The dissipation rate of the total energy is, by definition, $\epsilon^* + \chi_\rho^*$.

4.2. *Procedure for data analysis*

Depending on the distance downstream of the grid in terms of the mesh size, we selected from each run about 8 to 20 s of data in which stationarity of the time series was observed. It was important to carefully select data from those portions of the records when probes were in the working section, i.e. data unaffected either by acceleration and deceleration of the grid and the probe array and by tank-wall reflection. In most cases, the working section was no more than 40 % of the total length of the tank, or 7.2 m.

Statistical analyses were performed on the selected sections of the time series to obtain the mean values and mean squares in terms of the physical quantities of interest. For the velocity data, the two components had to be calculated from the signals of each pair of cross-film elements prior to the statistical analysis.

As discussed in §5, there exists a relatively low-frequency or long-wavelength component superposed onto the turbulence signals, which becomes apparent at large x/D. This component corresponds to a seiche motion set up in the tank due to the mean and start/stop motions of the grid. To reduce the contamination of this component to the turbulence signals, we adopted a running mean algorithm for calculating the mean square of the turbulence quantities. In essence, the entire time series was divided into sections of 500 data points. The mean square of the time series was estimated by ensemble averaging the mean squares of all the sections within the series. This algorithm effectively fed the signals through a high-pass filter. For a sampling rate of 833 Hz, the window width of the running mean algorithm is 0.60 s, which translates into a length of 24 cm for a towing speed of 40 cm s^{-1}. Comte-Bellot & Corrsin (1971) show that the integral scale in grid turbulence increases from $0.5M$ at $x/M \approx 50$ to $0.95M$ at $x/M \approx 400$. Here, the window width of the running mean algorithm is about $2.2M$. As a result, this high-pass filter with relatively low efficiency removes only an insignificant amount of energy in the energy-containing scales. However, the energy of the seiche motion, which has a wavelength of about 6 m (see §5), is significantly attenuated.

To estimate the system noise level, we conducted noise tests to measure the velocity components and density without the grid towed in the tank. The noise level, defined as the root-mean-square (r.m.s.) of the data divided by the mean value of the data, was calculated from the results of the noise tests. For the results presented in §5, we corrected all the mean squares by subtracting the corresponding mean squares derived from the noise tests. Such a correction is justifiable because the noise is mainly due to vibration of the towed carriage on which the hot-film probes were mounted (Liu 1992). In other words, the noise is linearly superimposed onto the signals and can be reasonably removed as described. It should be emphasized that the nature of the noise measured here is very different from the background noise in a wind or a water tunnel (Itsweire *et al.* 1986). For the velocity measurements, the noise levels are about 0.3 %, 0.13 % and 0.08 % for the longitudinal, lateral and vertical components, respectively. The noise level for the density measurements was too small compared to the signals to require correction. For example, the signal-to-noise ratio for density measurements for $F \approx 80$ at $x/D = 200$ is about 60. Consequently, no correction is required for the density data.

4.3. *Statistical errors*

For $x/M = 40$, we estimated the integral scale of the longitudinal velocity fluctuations to be about 4 cm. For a typical sampling time of 14 s, which corresponds to a sampling length of 560 cm, the number of independent samples is about 140. According to

Bendat & Piersol (1971), the normalized standard error for $(u^2)^{1/2}/U$ is 12%. Because the integral scale increases with increasing x/M, the standard error also increases proportionally with x/M. For $x/M \geqslant 200$, as the signal level approaches the noise level, the experimental error is expected to be abnormally large. Interpretation of the data for $x/M \geqslant 200$ should be made with care. In presenting the experimental results, we use error bars to represent the maximum spread of the data measured with the individual probes instead of the corresponding statistical errors. This is a reasonable way of providing an indication of the scatter of the data where an accurate estimate of the statistical errors cannot be easily made, especially for those quantities such as the dissipation rates that require multiple stages of operation on the experimental data.

5. Results

In this section, we present our experimental results in terms of the physical quantities that were defined in §4. These physical quantities are the (turbulence) kinetic, potential, and total energies and the dissipation of these energies. In addition, we derive a turbulence Froude number, an important parameter for turbulent stratified flows.

5.1. *Turbulence kinetic energy*

Figures 2(*a*)–2(*d*) show the kinetic energy versus downstream distance for $F \approx \infty$, 80, 40 and 20, respectively. The ordinate is the component of the kinetic energy $\overline{u^2}/U^2$, $\overline{v^2}/U^2$ or $\overline{w^2}/U^2$. The typical scatter of the data measured from the probes is represented by the error bars. We observe from figure 2(*a*) that the grid turbulence generated in the towing tank is not very isotropic. The ratio $\overline{w^2}/\overline{u^2}$ is about 0.6, whereas this ratio is about 0.8 for grid-generated turbulence in a wind tunnel with a straight duct (Comte-Bellot & Corrsin 1966).

Apparently a low-amplitude and low-frequency seiche motion is set up by towing the grid in the tank. A discussion of the cause and consequences of the seiche motion is given by Lange (1974). The seiche motion, which can be identified from the time series of the longitudinal velocity for large x/M, has a maximum amplitude of about $0.02U$ and a wavelength of about 6 m. The running-mean procedure was designed to remove most of this contribution to the longitudinal component of the kinetic energy. It is believed that such a contribution is larger for a smaller (shorter) towing tank because faster rates of acceleration and deceleration have to be used so that the grid will maintain a constant speed for a reasonable distance. Furthermore, the relatively low-frequency or long-wavelength seiche motion is a potential source of internal waves when the grid is towed in the vertical direction, as in the experiments of D & M.

Figure 2(*a*) shows that, for the non-stratified case, the components of the turbulence kinetic energy decrease with increasing downstream distance as $(x/M)^{-1.3}$. Deviation from the -1.3 power law is observed at large x/M ($\geqslant 200$), where the signal-to-noise ratio is near one. Interpretation of the results for $x/M \geqslant 200$ should be made with discretion. The straight lines fairing through the data points on the graphs show that our data are consistent with previous data obtained in wind tunnels (e.g. Comte-Bellot & Corrsin 1971). The turbulence intensity is slightly lower than that of the previous data due to the smaller geometric solidity of the grid used in the experiment (≈ 0.2). Note that the biplane grid used by Comte-Bellot & Corrsin had a solidity of 0.34.

The results shown in figure 2(*d*) were recalculated from the data originally measured by L & V using the analysis procedure described in §4. It should be pointed out that the turbulence intensity is noticeably reduced, compared to the original results (see Lin & Pao 1979), after subtraction of the noise level and removal of the seiche motion by the

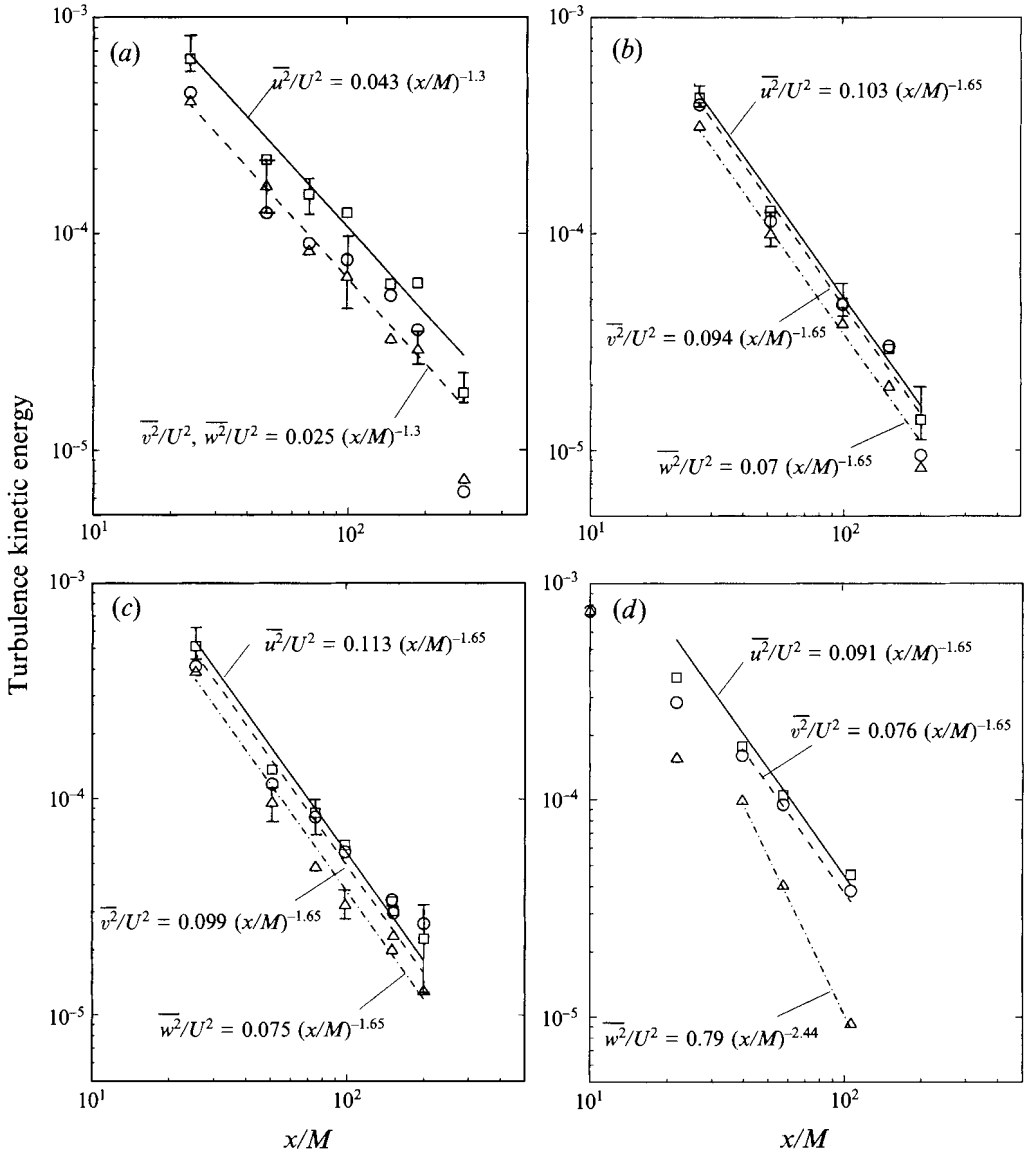

FIGURE 2. Decay of turbulence kinetic energy: (*a*) $F \approx \infty$, (*b*) $F \approx 80$, (*c*) $F \approx 40$, (*d*) $F \approx 20$ (experiments conducted by Lin & Veenhuizen (1974) using a single-plane grid with vertical elements): □, $\overline{u^2}/U^2$; ○, $\overline{v^2}/U^2$; △, $\overline{w^2}/U^2$. $U \approx 40$ cm s^{-1}.

running-mean procedure. Two important findings were derived from comparing the results in figures 2(*a*)–2(*d*). The first is the lower value and slightly larger decay rate of kinetic energy for the stratified cases than for the homogeneous case. Straight lines fairing through the data points show that the turbulence kinetic energy decays as $(x/M)^{-1.65}$ as compared with $(x/M)^{-1.3}$ for the homogeneous case. The generation of potential energy in the stratified wakes, which will be discussed later, accounts for the above. The second finding is the insignificant difference between the decay rates of the vertical and horizontal components of the kinetic energy for the homogeneous case and the stratified cases for $F > 20$. The decay rate of the vertical component, however, increases noticeably for $F \approx 20$, as can be seen from figure 2(*a*). (Owing to the low

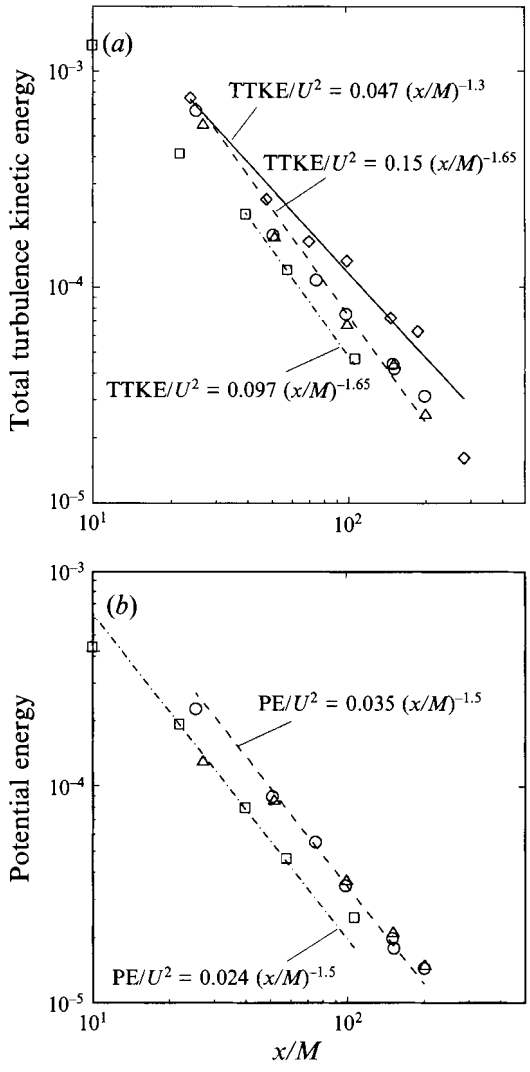

FIGURE 3. Decay of (*a*) total turbulence kinetic energy, (*b*) potential energy: □, $F = 20$ (L & V); ○, $F = 40$; △, $F = 80$; ◇, $F = \infty$.

solidity, the grid turbulence may not have been fully developed for $x/M < 20$.) The inhibition of the vertical motion by stratification is clearly demonstrated for the low Froude number run, $F \approx 20$.

It is clearly demonstrated in these figures that no abrupt transition is observed for any of the three stratified runs. Here, one may easily convert the abscissa from x/M to Nt by using the formula

$$Nt = (x/M)/F. \tag{23}$$

The much faster decay rate of the vertical kinetic energy for $F \approx 20$ is, in fact, opposite to the trend reported by D & M. Figure 3(*a*) displays the variation of the total (turbulence) kinetic energy with x/M. The straight lines fairing through the data points indicate that the kinetic energy decreases approximately as $(x/M)^{-1.3}$ for the homogeneous case and as $(x/M)^{-1.65}$ for the stratified cases, consistent with the

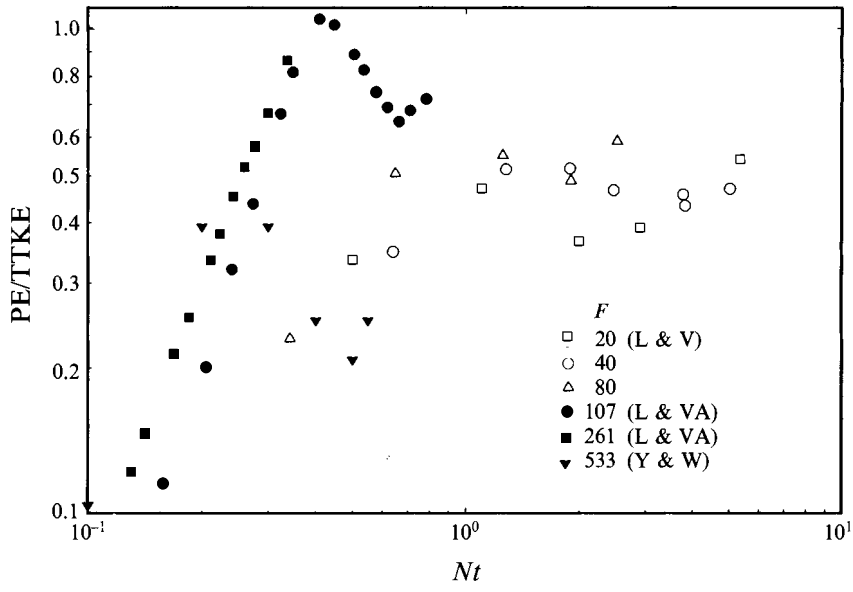

FIGURE 4. Ratio of potential energy to total turbulence kinetic energy.

individual components. For the present results, the total kinetic energy is about the same for all cases initially, as anticipated. The deficit in the kinetic energy is compensated for by the generation of potential energy in the stratified cases, as we shall see later (also see Riley *et al.* 1981). Within the accuracy of the measurement, it is not possible to resolve the difference in the total kinetic energy between the two stratified cases with $F \approx 80$ and 40.

5.2. *Potential energy*

The potential energy derived from the density measurements, as expressed in (8), is illustrated in figure 3(*b*). Comparison of figures 3(*a*) and 3(*b*) demonstrates clearly that the total kinetic energy is significantly higher than the potential energy, indicating that the energy is not equally divided into kinetic and potential energy for Nt as large as 5. This implies that, at least up to this point in time, the flow does not consist of a system of propagating internal waves. The potential energy decreases as $(x/M)^{-1.5}$ for all the stratified cases. The vertical component of the kinetic energy tends to be higher initially and becomes lower than the potential energy, as can be seen by comparing figure 3(*b*) with figures 2(*b*)–2(*d*). Such a trend is especially evident for $F \approx 20$. Initially, the turbulence energy generated by the grid is almost totally kinetic. Subsequently, part of the kinetic energy is converted into potential energy. At large Nt (e.g. much greater than 5), the turbulent motion in the vertical direction has been significantly affected by stratification. The ratio of PE to TTKE, estimated from figure 3, is plotted in figure 4 as a function of Nt for $F \approx 20$, 40 and 80.

The scatter in the data is not too large, even though the results were derived from experiments using two different grids. Furthermore, oscillations in the potential and kinetic energies (Riley *et al.* 1981) increase the scatter of the data. The data in figure 4 show that the ratio of PE to TTKE increases with increasing Nt. The rate of increase, however, decreases with increasing Nt. From the three data sets, the ratio of PE to TTKE is about 0.2 at $Nt \approx 0.3$, tapering off to about 0.5 at $Nt \approx 5$. The trend of the data indicates an asymptotic ratio of about 0.5. Based upon the decomposition suggested in Riley *et al.* (1981), the asymptotic ratio thus indicates that about one-third

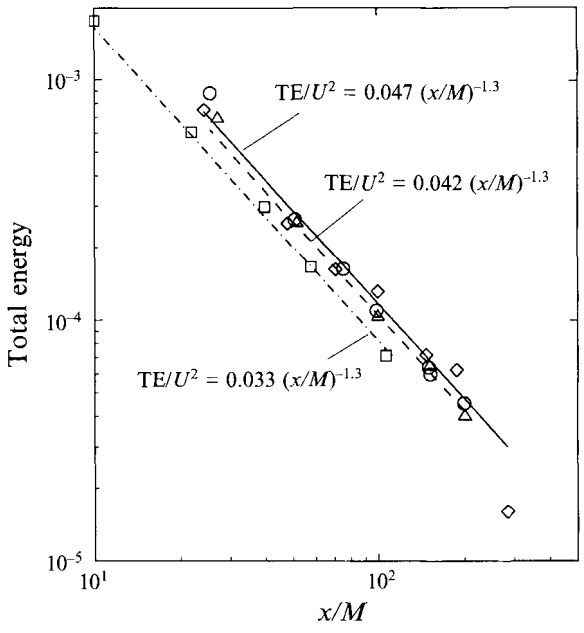

FIGURE 5. Decay of total energy. Symbols as figure 3.

of the total energy is in quasi-horizontal motion and two-thirds is in internal waves. These values agree reasonably well with those derived from direct numerical simulations (Riley *et al.* 1981).

For comparison, the ratios for the low-F cases of Lienhard & Van Atta (1990) and Yoon & Warhaft (1990) (referred to herein as L&VA and Y&W respectively) obtained in stratified wind tunnels are plotted as solid symbols in figure 4. Their data only extend to $Nt < 0.8$ within which the ratios show a clear oscillatory trend. The buoyancy time is simply too short to demonstrate whether an asymptotic ratio is established. From the small overlapping region, the trend of the present results seems to be more consistent with that of Y & W than that of L & VA. There are discrepancies in the peak ratio and the time at which the peak occurs between the two sets of wind-tunnel data, with the peak ratio of L & VA reaching slightly higher than unity at $Nt \approx 0.4$ and that of Y&W being around 0.4 between $Nt \approx 0.2$ and 0.3. According to Y & W, the exact cause of the discrepancies is unclear but is likely due to the difference in the initial conditions. (For the low-F cases of L & VA, the buoyancy effects become important very close to the grid before the grid turbulence is fully developed. In addition, the initial temperature fluctuations are higher in the experiments of L & VA (± 0.3 °C) than those of Y & W (< 0.1 °C).)

5.3. *Total energy*

Figure 5 shows the total (turbulence) energy, the sum of the kinetic and potential energies, as a function of x/M. For the homogeneous case, the total kinetic energy is the total energy, because there is no potential energy. For all three cases considered in the present investigation, the total energy is practically identical within the accuracy of the measurements. For all cases, the total energy manifests the $(x/M)^{-1.3}$ power law, which is the same as that for the homogeneous case. The equality of the total energy indicates that the effect of the stratification, from the energy point of view, is simply to convert kinetic energy to potential energy, although the detailed dynamics of the

homogeneous and stratified flow fields are very different. This finding is, of course, nothing more than the law of conservation of energy. Up to this point, the laboratory results are very consistent with the predictions by Riley *et al.* (1981).

5.4. *Dissipation rates*

Figure 6(*a*) illustrates the dimensionless kinetic energy dissipation rate, $\epsilon M/U^3$, as a function of x/M. For all cases, the dissipation rate tends to decrease as $(x/M)^{-2.3}$, as shown by the straight lines fairing through the individual data points for $x/M < 200$. This power law is consistent with the power law of the kinetic energy in a homogeneous fluid because

$$-\epsilon \propto \frac{\overline{\mathrm{d}u^2}}{\mathrm{d}t} \propto \frac{\mathrm{d}}{\mathrm{d}t}\left(\frac{x}{M}\right)^{-1.3} \propto \left(\frac{x}{M}\right)^{-2.3}. \tag{24}$$

By and large, when the same grid was used, the dissipation rate was larger for the homogeneous case than for the stratified cases. According to Riley *et al.* (1981), the decrease in the dissipation of kinetic energy is almost compensated for by the dissipation of potential energy.

Also shown are the dissipation rates for the two most stable cases of L & VA. Reasonable agreement among the data sets is observed, except for the slightly steeper roll-off seen in L & VA's data. The steeper roll-off is consistent with the high values of the PE/TKE ratio, as PE builds up at the sacrifice of TKE (figure 4).

The potential dissipation was derived from the spectrum of the density fluctuations by using (19) and (20) whenever a Batchelor subrange existed (see §4 for discussion). Figure 6(*b*) shows the dissipation rate of the potential energy. Comparison of figures 6(*a*) and 6(*b*) demonstrates that the potential dissipation, which follows the same power law, is lower than the kinetic energy dissipation. Asymptotically, the corresponding results of L & VA follow approximately the same power law for $F \approx 107$ and 136, but the magnitudes are lower than those of the present results. The initial deviation from the asymptotic roll-off in L & VA's data is an indication of the non-equilibrium state of the flow at small x/M.

Figure 6(*c*) shows a comparison of the total energy dissipation (kinetic and potential) for the stratified and homogeneous cases. Considering the data scatter and the uncertainty of the value of β (a value of 3.0 is used here) in (19), it is not possible to distinguish the total energy dissipation rate for $F \approx 40$, 80 and ∞. The agreement between L & VA's data and the present results also improves when we compare the total energy dissipation rate.

5.5. *Turbulence Froude number*

At this point, it is appropriate to introduce an important dynamic parameter for turbulent stratified flows. From the ratio of inertial to buoyancy forces, we can derive a turbulence Froude number, F_T, on dimensional grounds (Riley *et al.* 1981):

$$F_T = (\overline{u^2})^{1/2}/(Nl), \tag{25}$$

where l denotes the integral scales of the velocity field. From a physical point of view, the flow is turbulent-like for $F_T \gg 1$ and is internal-wave-like for $F_T \ll 1$. In turbulent flows,

$$l = (\overline{u^2})^{3/2}/\epsilon. \tag{26}$$

From (25) and (26), we have

$$F_T \approx \epsilon/(\overline{u^2}N). \tag{27}$$

When we substitute the results obtained from a homogeneous fluid, $\overline{u^2} \propto (x/M)^{-n} \propto t^{-n}$ and $\epsilon \propto (x/M)^{-n-1} \propto t^{-n-1}$, then (27) becomes

$$F_T \approx A(Nt)^{-1}, \tag{28}$$

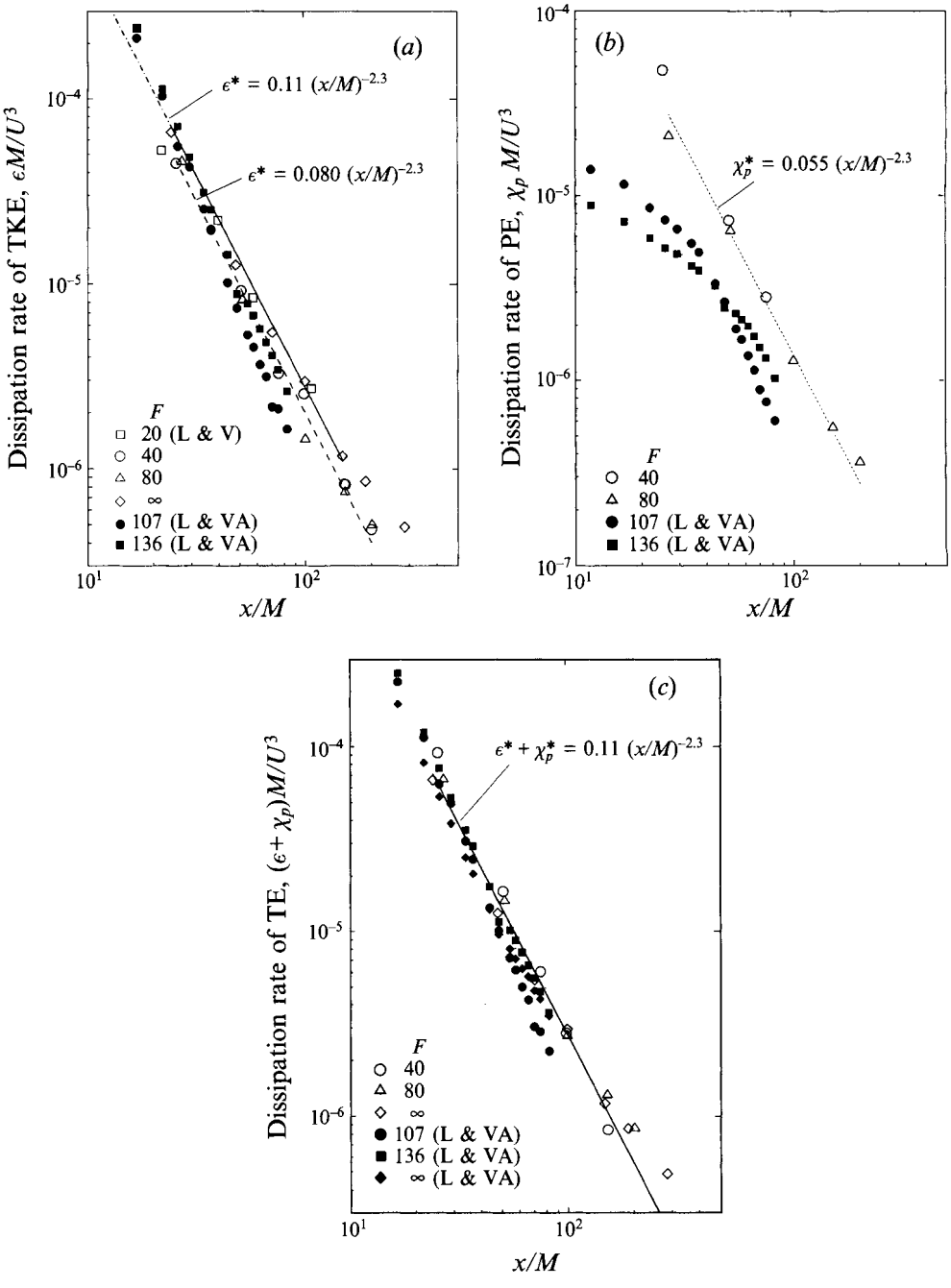

FIGURE 6. Decay of dissipation rate of (*a*) turbulence kinetic energy, (*b*) potential energy, (*c*) total energy.

where A is a constant of order one. In a stratified fluid, Riley *et al.* (1981) suggested an alternative representation of F_T:

$$\hat{F}_T = \frac{\text{Dissipation of total energy}}{\text{Total energy} \times N}. \tag{29}$$

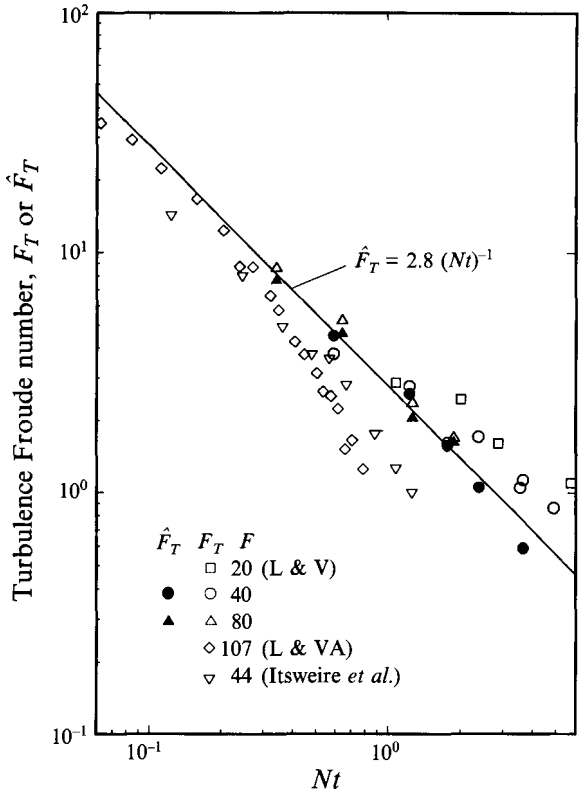

FIGURE 7. Decay of turbulence Froude number.

Equation (29), which is similar to (27), takes into consideration the additional potential dissipation in a stratified fluid. Figure 7 is a plot of F_T and $\hat{F}_T$ as a function of Nt for $F \approx 80$, 40 and 20. The solid symbols show that $\hat{F}_T$ tends to collapse onto a single curve: it follows $(Nt)^{-1}$ very well for $Nt < 2$ and then decays faster than $(Nt)^{-1}$ for $Nt > 2$. Here, only those data for which the potential dissipation can be estimated according to (19) and (20) were plotted. The open symbols show that there is considerable scatter in F_T: it tends to be higher for $F \approx 20$ than for $F \approx 40$ and 80, probably due to the different configurations of the grids. For the present experiments, $\hat{F}_T \approx 1$ for $Nt \approx 2$, and $\hat{F}_T$ is about 0.5 even as late as $Nt = 5$, which is not yet low enough for the flow to be totally dominated by stratification. Consequently, we anticipate that the flow is at least weakly turbulent for $Nt \approx 5$. At that time, we expect that many turbulent patches are present and are affecting the flow field. Note that the ratio of $F_T/\hat{F}_T$ is roughly 1.2.

The corresponding results of L & VA for $F \approx 107$ and those of Itsweire *et al.* (1986) for $F \approx 44$ (R37) are also plotted in figure 7. All the data sets follow the $(Nt)^{-1}$ trend well initially. At large Nt, the present data fall off less rapidly than do the others. One possibility is that, at large Nt, stratified turbulence generated by a towed grid in a towing tank without background turbulence is more patchy than that generated by a stationary grid in a water or wind tunnel, in which weak background turbulence is present. Particularly at very large Nt, the effect of the difference in the Schmidt number and the Prandtl number may play an important role in the persistence of the patchy formation, as we shall discuss later.

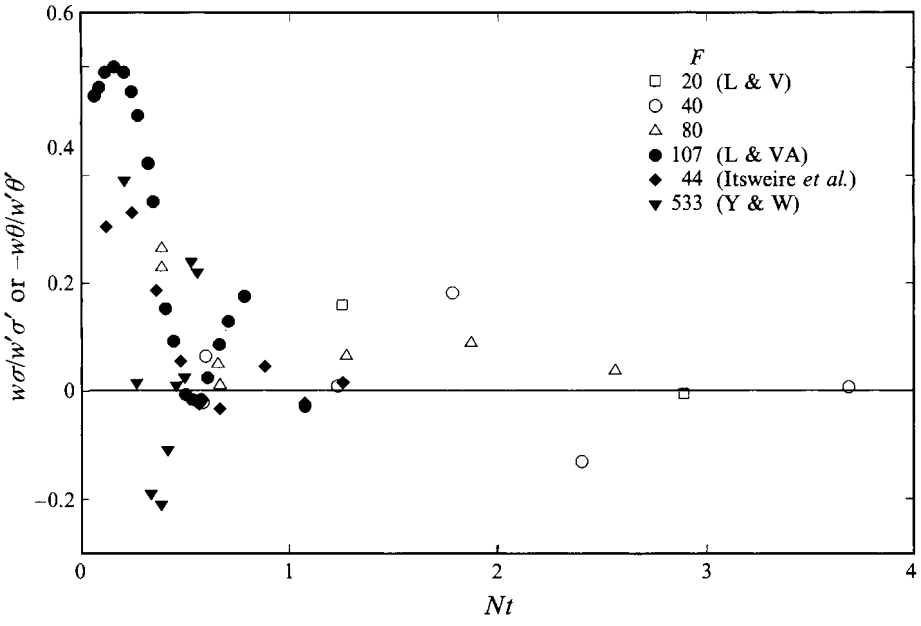

FIGURE 8. Evolution of buoyancy flux.

5.6. *Buoyancy flux*

Figure 8 illustrates the evolution of the buoyancy flux, $\overline{w\sigma}/\overline{w'\sigma'}$ with Nt for $F \approx 20$, 40 and 80. For comparison, we also plot selected sets of $-\overline{w\theta}/\overline{w'\theta'}$ from L & VA for $F \approx 107$, Itsweire *et al.* (1986) for $F \approx 44$ (R37) and Y & W for $F \approx 533$. The Nt or x/M spacing in the present data is too coarse to track the oscillation of the buoyancy flux, as demonstrated by the numerical simulation of Métais & Herring (1989). A similar trend is observed for most of the laboratory data sets except for that of Y & W with F much higher than those of the rest. The buoyancy flux of Y & W not only displays clearly the countergradient flux but also reaches the first zero crossing sooner than do the others. According to Y & W, the presence of initial background temperature fluctuations tends to reduce the countergradient buoyancy flux. Note that the present results extend to much larger Nt than the others, one of the advantages of the towing tank. The relatively coarse spacing between data points, however, may have missed the region in which countergradient flux takes place.

5.7. *Effect of high Schmidt number*

As mentioned earlier, one of the main differences between stratified turbulence generated in salt water and in air is that the Schmidt number of the former (≈ 500) is about 3 orders of magnitude higher than the Prandtl number of the latter (≈ 0.7). The fact that the Prandtl number is close to unity indicates that the Kolmogorov dissipation scale is the same as the thermal dissipation scale in air and there is only one microscale to consider. In salt water, the mass dissipation scale is much smaller than the Kolmogorov dissipation scale, and we may have to consider one additional microscale. Some of the discrepancies between the turbulence characteristics measured in the two media may be attributed to the above difference, especially at large Nt when turbulence has been largely dissipated. If there is a mechanism that generates two-dimensional or quasi-two-dimensional density fine structure in the two media, such fine

structure is expected to persist much longer in stratified salt water than in thermally stratified air.

To investigate the effect of large Schmidt numbers on the evolution of stratified turbulence, two-dimensional density fine structure was generated by towing a horizontal array of thin strings in the towing tank. Several strings 2 mm in diameter with vertical separations of 2 or 3 cm between strings were stretched tightly between two thin struts that spanned the tank width and were mounted on one of the oil-bearing carriages. The array of strings was towed at a range of speeds from 5 to 10 cm s^{-1} in the stratified salt water with a range of B–V frequencies. The above parameters were varied to optimize the generation of density fine structure, consisting of alternating layers of strong and weak density gradients in the otherwise stratified fluid with a constant B–V frequency. The evolution of the wakes generated by passage of the strings was monitored visually with shadowgraphs and quantitatively with measurements of density profiles using vertically plunging conductivity probes (see §3). The probe speeds were 20 cm s^{-1} at small times and 10 cm s^{-1} at large times.

Figure 9 shows side views of a series of shadowgraph pictures of the wakes generated by the strings. The number below each picture is the time in seconds after passage of the strings with reference to the centre of the shadowgraph picture. In this case, there were six strings with a vertical separation of 2 cm. The towing speed was 5 cm s^{-1}, and the B–V frequency was 0.09 Hz. The Reynolds and Froude numbers based on the diameter of the strings were $R_d = 100$ and $F_d = 278$. Just after passage of the strings, at 1.6 s ($Nt \approx 0.14$), the wakes trailing the individual strings are clearly identifiable. Upstream of the struts, the relatively uniform brightness of the shadowgraph indicates that the undisturbed fluid has a constant density gradient. Initially, the wake height grows rapidly and reaches its maximum a short distance downstream of the strings. Inside the wakes, intensive mixing is evident. In between the wakes, bright layers that are thinner than the wakes emerge, indicating the formation of thin sheets of strongly stratified fluid. Only limited mixing takes place in the regions between the wakes. As fluid particles that are heavier or lighter than the ambient are entrained from below or above into the between-wake regions and mixed partially with the ambient, most of them do not have sufficient kinetic energy to overcome the stratification and are trapped within these regions. As a result, the gradient in these regions increases accordingly.

A relatively mild collapse of the two-dimensional wakes is evident, unlike the collapse of a cylindrical wake (Lin & Pao 1979). From the movie record of the experiments, we detect the undulation of the layers as a whole. Relatively isotropic microstructure, with a scale finer than that of the fine structure, is observable inside the wakes up to about 80 s ($Nt \approx 7$), indicating that there is residue of turbulence in the weakly stratified layers even at such a large buoyancy time. The vanishing of this microstructure as time increases is clearly illustrated in the picture series. Non-isotropic microstructure beings to appear at about 30–40 s ($Nt \approx 3$), indicating the formation of small-scale internal waves. Very little activity is observed inside the wakes beyond 140 s ($Nt \approx 12$). Radiation of internal waves from the disturbed flow region into the undisturbed region takes place as early as 20 s ($Nt \approx 1.8$) after passage of the strings, and long after small-scale activities in the wakes vanish ($Nt \approx 30$). These long-crested short internal waves (< 1 cm) are most visible just above the top of the disturbed region from 40 to 280 s ($Nt \approx 3.8$ to 25). The two-dimensional pattern of the fine structure becomes most distinctive around 140 s ($Nt \approx 12.6$), after which the optical contrast of the sheet-layer pattern and, therefore, the distinction between the strongly stratified sheets and the weakly stratified layers deteriorates gradually. However, the

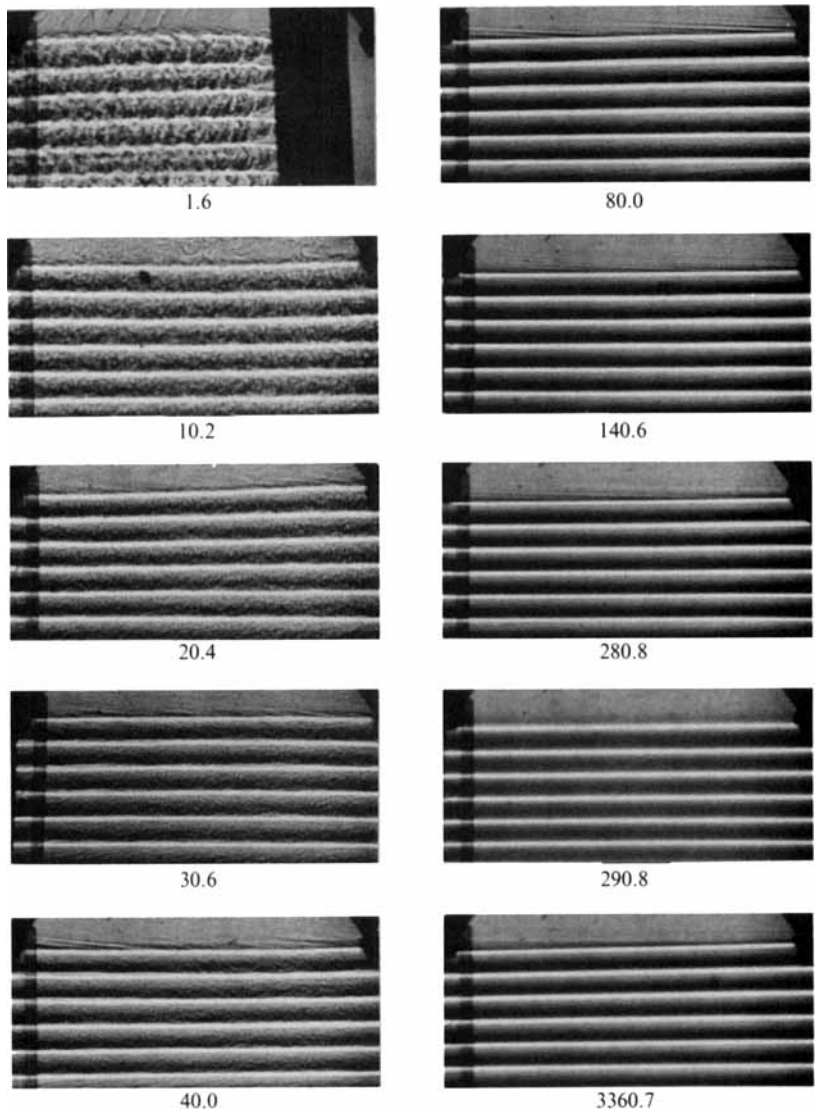

FIGURE 9. Shadowgraph pictures showing the evolution of two-dimensional density fine structure generated in the wakes of a horizontal string array. The numbers below each picture show the time in seconds after passage of the strings.

same pattern is still distinguishable long after 3000 s ($Nt \approx 270$). In fact, this pattern persists for several hours before it vanishes completely.

Figure 10 shows several vertical density profiles measured with an array of vertically plunging conductivity probes after passage of the strings. The abscissa and the ordinate are the reduced density and the vertical distance, respectively. The abscissa is shifted one division for each subsequent density profile. In this case, a total of 12 strings with a vertical separation of 3 cm was used. The towing speed and the B–V frequency were 10 cm s^{-1} and 0.09 Hz. The corresponding Reynolds and Froude numbers were $R_d \approx 200$ and $F_d \approx 560$. The earliest profile was measured at 13 s ($Nt \approx 1.2$). The profile shows no trace of any two-dimensional fine structure, in contrast to those displayed in figure 9. Instead, there are regions in which the density gradient is locally unstable but

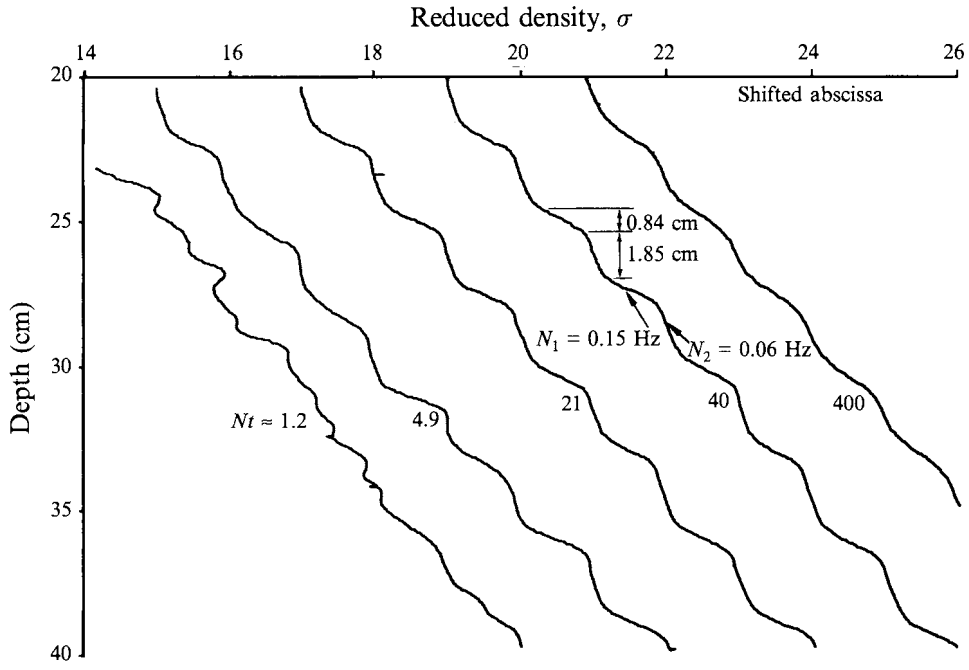

FIGURE 10. Density profiles in the wakes of a horizontal string array towed in a stratified salt-water with a constant density gradient. String diameter 2 mm, string separation 3 cm, towing speed 10 cm s^{-1}, $N = 0.09$ Hz.

the profile is stable overall. The presence of these unstable regions indicates local overturning of the stratified fluid as a result of turbulent mixing. The above characteristics are quite different from the shadowgraph observation in that the two-dimensional density pattern is established at the very beginning during passage of the strings. Note that the density profiles represent thin cuts through the corresponding shadowgraph pictures, which are integrated over the entire width of the tank. The combined results of the density profiles and the shadowgraph pictures indicate that the flow field generated by the towed strings is basically two-dimensional, although individual realizations are not. From the density profiles, the two-dimensional pattern of density fine structure begins to form shortly after $Nt \approx 1.2$ and becomes very distinctive at 54 s ($Nt \approx 4.9$) and beyond. The sharpness of the pattern peaks at around $Nt \approx 20$–40 and deteriorates thereafter. On average, the maximum B–V frequencies are 0.15 Hz for the strongly stratified sheets and 0.06 Hz for the weakly stratified layers, as compared to 0.09 Hz for the undisturbed fluid. The corresponding thicknesses of the sheets and layers are 0.8 and 1.9 cm. It is interesting to point out that the separation between the sheets or layers is less than that between the strings. Apparently, the disturbed region as a whole experiences a slight collapse that contributes to the relatively small separation of the sheets or layers. At $Nt \approx 400$, the pattern is still distinctive, with the density gradients of the sheets decreasing and those of the layers increasing, respectively.

The above generation mechanism, which is conceptually illustrated in figure 11, is expected to occur in three-dimensional flows. The two-dimensional pattern of the fine structure, however, persists much longer than that of the three-dimensional counterparts. In fact, the persistence of the two-dimensional pattern is comparable to the characteristic diffusion time due to molecular motion (10^5 s for a 1 cm thick layer

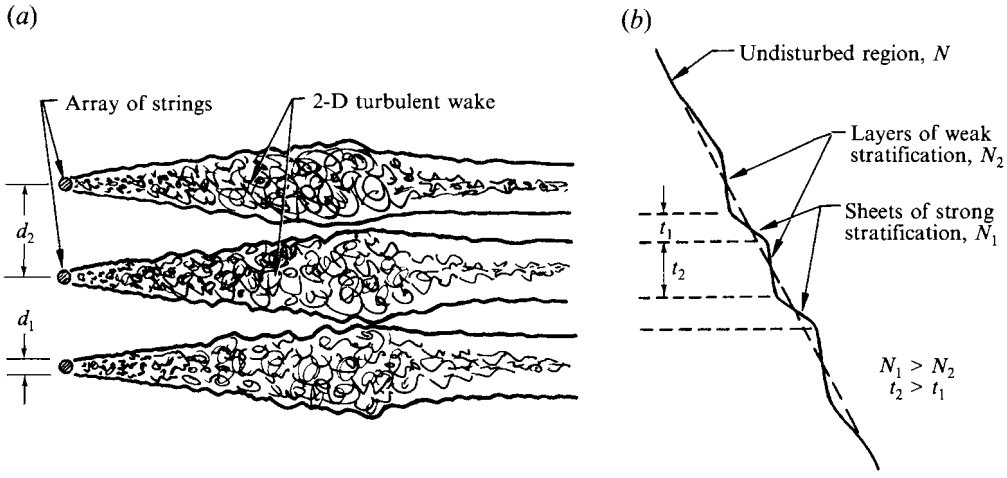

FIGURE 11. Conceptual drawing of the generation and evolution of density fine structure: (*a*) schematic of stratified wakes (side view), (*b*) vertical density profile.

of NaCl concentrate, as estimated by Lange 1974). In contrast, three-dimensional fine structure tends to persist on the order of 10^2 s (Lange 1974). In the three-dimensional case, sheets and layers are distributed non-uniformly in space. This non-uniform distribution creates horizontal density gradients (not present in the two-dimensional case) that are capable of smoothing out density fine structure. Furthermore, turbulence is sustained longer in weakly stratified layers than in strongly stratified sheets. As a result, patches of turbulence in layers of weak stratification coexist with strongly stratified sheets in which turbulence has been suppressed. When the turbulent patches are brought into contact with the strongly stratified sheets, the sheets are destroyed by turbulence. Consequently, the effective diffusivity is higher than the molecular diffusivity and is responsible for Lange's estimate. Therefore, in a stratified water tunnel with background turbulence, the fine structure is expected to be less persistent than in a towing tank with a quiescent background.

The above description is physically consistent with measurements conducted in the ocean thermocline, where patches of turbulence have been constantly identified (Gregg 1980). In the ocean environment, the Reynolds number is several orders of magnitude higher than that attainable in the laboratory. Even in strongly stratified layers, turbulence may be generated locally at places where strong current shear is present and is responsible for the relatively short persistence of three-dimensional ocean density fine structure.

In the stratified wake of an axisymmetric body, Lin & Pao (1979) demonstrated the development of large-scale 'pancake' vortices that persist for a very long time. The vortex formation is the result of the unstable quasi-two-dimensional flow developed in the wake after the wake collapses. At the wake edges, particularly near the top and bottom, partial mixing between the ambient and the turbulent fluid in the wake may lead to the generation of quasi-two-dimensional fine structure similar to that observed above, as confirmed by vertical density profiles measured with the plunging probes (not shown). Subsequently, the fine structure is entrained into the wake by the vortex motion and evolves into the vertically staggered 'pancake' formation.

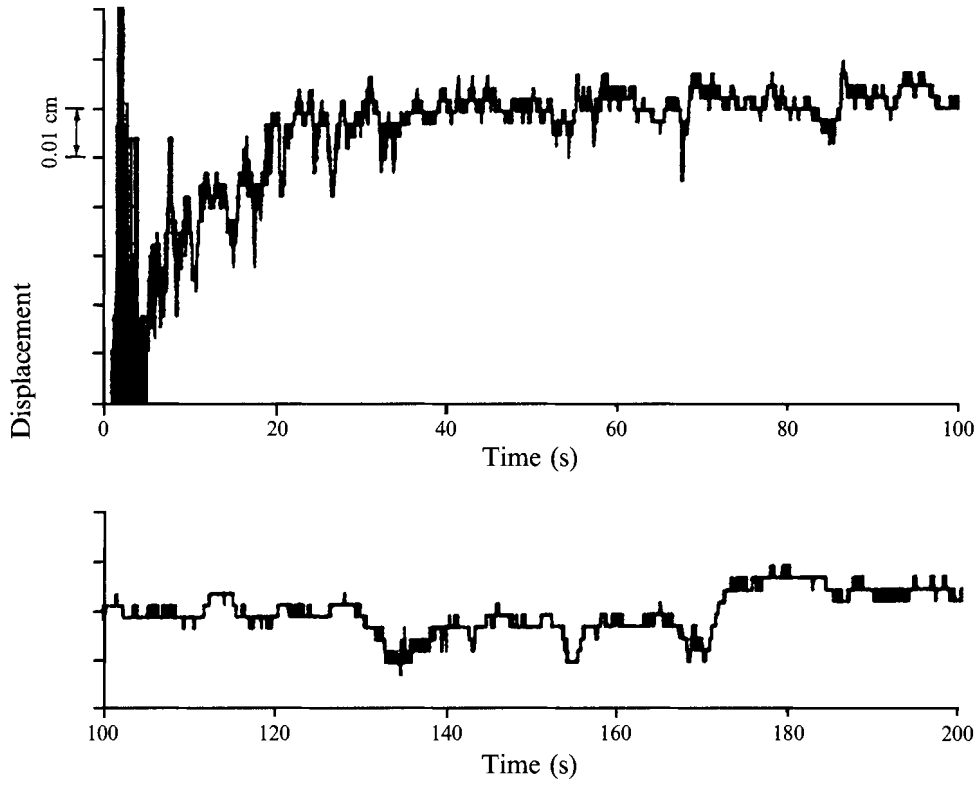

FIGURE 12. Vertical displacement of stationary optical interface in a turbulent stratified fluid. $F \approx 60$.

6. Discussion

The present results agree, at least qualitatively, with all the findings of Riley *et al.* (1981) derived from direct numerical simulations of homogeneous turbulence in a density-stratified fluid. All these results, together with those obtained by Britter *et al.* (1981) and Itsweire *et al.* (1986), have a different trend than those of D&M, who reported an abrupt change in the decay rate of turbulence kinetic energy, whereas the others show no such change at large x/M.

Van Atta *et al.* (1984) attributed the above discrepancy to the fact that two different classes of measurements were actually taken, depending on the presence and intensity of internal waves when the turbulence was being generated by the grid. Class I data are relatively free of internal waves near the grid (L&V; Britter *et al.* 1981 and Itsweire *et al.* 1986), and Class II data have strong internal waves near the grid (D&M and Stillinger *et al.* 1983). In view of the low initial PE/TTKE from figure 4, the present results belong to those of Class I. Van Atta *et al.* (1984) suggested that the abrupt change in the decay rate of the turbulence kinetic energy observed in the Class II data could be wrongly interpreted if the presence of slowly decaying internal-wave components is not accounted for throughout the evolution of the turbulence. This view is supported by the finding that PE/TTKE increases with time (figure 4). For Class II measurements, the initial PE/TTKE is high, and the asymptotic ratio may reach unity as the result of the relatively slow dissipation of internal-wave motion. In other words, after the turbulence is dissipated, the residue motion is essentially that of the internal

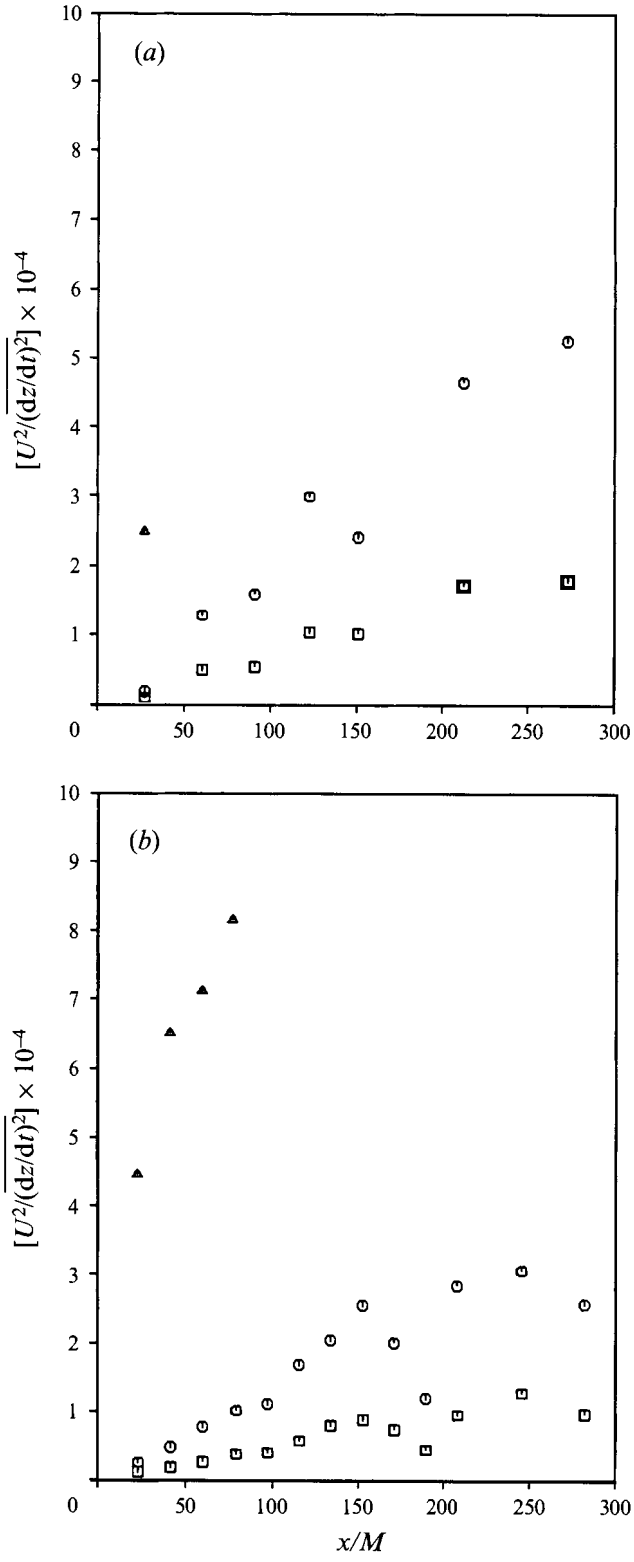

FIGURE 13. Decay of vertical apparent velocity in a turbulent stratified fluid: (*a*) $F \approx 60$, (*b*) $F \approx 41$. Low-pass filtered results: ⊡, 400 Hz; ⊙, 200 Hz; △, 100 Hz.

waves. An attempt was made by Itsweire *et al.* (1986) to separate the velocity fluctuations of the wave components from those of the turbulence components in the data of Stillinger *et al.* (1983). With the wave components separated, the decay rate of the turbulence intensity of the vertical velocity component increases significantly, and the apparent abrupt change in the decay rate disappears.

In addition to the suggestion by Van Atta *et al.* (1984) that the measurements of D & M belong to those of Class II with strong internal waves near the vertically plunging grid, there appear to be other plausible factors contributing to the abrupt change observed in the decay of the turbulence kinetic energy. First, the exposure time of their photographic technique increased exponentially with time to maintain a particle tracelength of 0.2 to 4.0 cm. The corresponding exposure time is therefore in the range of 0.4 to about 10 s between $x/M = 300$ to 600. The relatively long exposure time excluded the high-frequency components of the velocity fluctuations.

The second factor pertains to the use of an optical method in a turbulent stratified fluid where the signals are contaminated by the apparent motion of the tracer particles as a result of fluctuations in the refractive index. The velocity fluctuations measured by the optical method may be caused predominantly by the optical distortion induced by the fluctuation of the refractive index in the turbulent, density-stratified water, especially long after the turbulent motion of the fluid particles is damped significantly by stratification. In fact, this has been studied to estimate the 'jitter' of stellar images observed through telescopes (Monin & Yaglom 1975) and to determine the displacement fluctuation of a laser spot (Yokoi 1982) in the lower atmosphere.

To demonstrate that such is the case, a separate series of experiments was conducted to measure the apparent velocity fluctuations of a stationary object in the same stratified grid-turbulence field used in the present investigation. In essence, the apparent displacement of a stationary optical interface in the stratified wake of the biplane grid was measured with a self-scanning photodiode array housed in the focal plane of a camera (Reticon Corporation, Model LC600V). The interface was created by a straight edge of Plexiglas plate illuminated from behind with a diffusive light source. A detailed description of the Reticon camera is given in Liu & Lin (1982). The apparent velocity was derived by time differentiation of displacement signals (figure 12). The signals were first smoothed using digital filtering. The quantization noise resulting from the finite spatial resolution of the diode array was derived from a noise test conducted in a quiescent stratified fluid. It was then subtracted from the apparent velocity derived from the data measured in the wake of the grid.

The most relevant results are shown in figures 13(*a*) and 13(*b*). In the ordinate $\mathrm{d}z/\mathrm{d}t$ is the first time differencing of the vertical displacement giving the vertical apparent velocity of the stationary object (the optical interface created by the straight edge). The corresponding Froude numbers for the two figures are 60 and 41. In each figure, results for the 100, 200 and 400 Hz low-pass filters are shown. Comparison of the two figures indicates that the apparent velocity fluctuation increases with decreasing F, as expected. In both figures, the dramatic effect of the low-pass filtering is evident. It should be pointed out that D & M used an exponentially decaying voltage to regulate the frequency of a chopping wheel, which controls the sampling frequency. After one B–V period, the sampling frequency is no more than a few Hertz because $(w^2)^{1/2}/(\text{minimum trace-length}) \approx (0.5\ \text{cm s}^{-1})/(0.2\ \text{cm}) \approx 2.5$ Hz, as estimated from the information reported by D & M (§§ 3 and 4). Owing to the low sampling frequency, the estimated kinetic energy is expected to be low as a result of the exclusion of high-frequency components.

The results presented in figure 13 were measured optically and may be directly

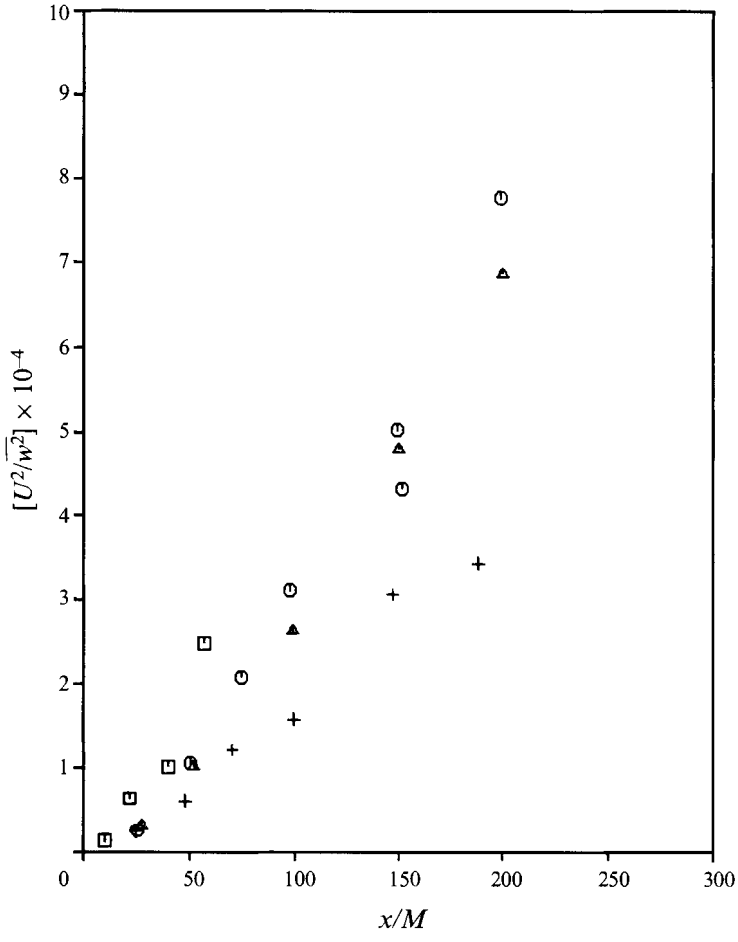

FIGURE 14. Decay of $U^2/\overline{w^2}$, inverse of the vertical component of the turbulence kinetic energy: □, $F \approx 20$ (L & V); ○, $F \approx 40$; △, $F \approx 80$; +, $F \approx \infty$.

related to those of D & M. The trend of an abrupt change in the decay of the vertical component of the turbulence kinetic energy is demonstrated in the two figures, particularly for the low-F case, consistent with that reported by D & M.

To assess the effect of the apparent velocity induced by the density fluctuations on the optical method used by D & M, the inverse of the vertical components of the turbulence kinetic energy, $U^2/\overline{w^2}$, is plotted in figure 14. It is evident that the vertical component of the turbulence kinetic energy is largest in the homogeneous fluid ($N = 0$) in the absence of the potential energy.

For convenience, let us examine the 200 Hz low-pass results, which are reasonably smooth and yet retain most of the high-frequency information. Note that the maximum vertical component of the turbulence kinetic energy (plusses in figure 14) is at most equal to the corresponding values of the apparent velocity (circles in figure 13); in other words, the former could be overwhelmed by the latter for low F. Because F is about 8 to 5 times higher in D & M's experiment than in the present experiment, the effect of the apparent velocity would be weaker, particularly at small x/M. At large x/M, after the grid-generated turbulence has been mostly dissipated, the effects of the apparent velocity and of the internal waves (Van Atta *et al.* 1984) would become

increasingly important, and the combined effects could lead to a non-decaying field. Therefore, the effects of the fluctuations in the refractive index must be taken into consideration in interpreting results measured in a stratified fluid using optical methods such as particle imaging velocimeters.

7. Conclusions

In this paper, we have presented detailed tow-tank measurements of the turbulence kinetic and potential energies in the stratified wake of a biplane grid for $F \approx \infty$, 80 and 40. To extend the data set to a lower Froude number ($F \approx 20$), we also included data of L & V, who used a single-plane grid with only vertical elements. We examined and compared the decay properties of the kinetic and potential energies and the dissipation rates for the respective components and for the sum of the components in order to determine the effects of stratification on grid turbulence. Comparison of our results and others from salt-water and wind-tunnel experiments generally shows a similar trend with few exceptions. The most important findings are summarized below.

(i) The decay rates of the energy and of the dissipation rates all follow a power law ($x/M < 200$). For the turbulence kinetic energy TKE, $(\overline{u^2}/U^2, \overline{v^2}/U^2) \propto (x/M)^{-n_1}$ and $(\overline{w^2}/U^2) \propto (x/M)^{-n_2}$, where $n_1 = 1.3$ for $F \to \infty$ and 1.65 for $20 < F \leqslant 80$, and $n_2 = 1.65$ for $20 < F \leqslant 80$ and 2.44 for $F \approx 20$. For the total kinetic energy, TTKE $= \overline{q^2}/2 \propto (x/M)^{-n_3}$, where $n_3 = 1.3$ for $F \to \infty$ and 1.65 for $20 < F \leqslant 80$. For the potential energy, PE $\propto (x/M)^{-1.5}$ for $20 < F \leqslant 80$. For the total energy, TE $\propto (x/M)^{-1.3}$ for all F. For the dissipation rate of the kinetic energy, $\epsilon \propto (x/M)^{-2.3}$ for all F. For the dissipation rate of the potential energy, $\chi_\rho \propto (x/M)^{-2.3}$ for all $40 \leqslant F \leqslant 80$ and $Nt \leqslant 2$. For the total dissipation rate, $\epsilon + \chi_\rho \propto (x/M)^{-n_4}$, where $n_4 = 2.3$ for $F \to \infty$. Accurate determination of n_4 for the stratified cases cannot be made from our data because of the assumptions involved in deriving the dissipation rate of the potential energy.

(ii) One of the stratification effects is to promote the decay rate of the kinetic energy, especially the vertical component for $F \approx 20$. The faster decay rate is, however, almost totally compensated for by the production of potential energy.

(iii) The vertical component of the kinetic energy tends to be higher initially and then becomes lower than the potential energy at large Nt. The ratio of the potential energy to the total turbulence kinetic energy increases from about 0.2 at $Nt \approx 0.3$ to about 0.5 at $Nt \approx 5$. The rate of increase of the ratio, however, decreases with increasing Nt. The asymptotic value of the ratio is not expected to be much greater than 0.5 from the trend of the data. According to the criterion of Van Atta *et al.* (1984), the present experiments belong to those of Class I which is free of internal waves near the grid.

(iv) The turbulence Froude number, F_T or $\hat{F}_T$, an important dynamic parameter for turbulent stratified flows, is $\hat{F}_T \approx 2.8\,(Nt)^{-1}$ for $Nt < 2$. $\hat{F}_T$ is about 0.5 as late as $Nt \approx 4$, indicating that the flow is not yet totally dominated by stratification. Consequently, the flow is at least weakly turbulent at $Nt \approx 4$, and the turbulence is probably patchy. Typical values of F_T obtained in a stratified water or wind tunnel follow the same $(Nt)^{-1}$ trend initially but tend to fall off more rapidly at large Nt.

(v) Two-dimensional fine structure consisting of alternating strongly stratified thin sheets and weakly stratified layers was generated by a towed array of thin strings in the towing tank. The thin sheets with density gradients larger than the undisturbed fluid were formed between the wakes of the strings, where mixing is localized and incomplete. In stratified salt water with a Schmidt number of about 500, the fine structure persists beyond several hundred B–V periods. Quasi-two-dimensional fine

structure, which may be linked to the 'pancake vortices' observed in the late wake of an axisymmetric body (Lin & Pao 1979), also persists until a very large buoyancy time. In a thermally stratified wind tunnel with a Prandtl number of about 0.7, strongly stratified sheets, if generated, are not expected to persist owing to the comparatively large thermal diffusivity. In a stratified water or wind tunnel, where background turbulence is present, the persistent of fine structure is expected to reduce accordingly.

The author wishes to thank Professor R. R. Long and Drs J. J. Riley and J. C. Schedvin for reviewing this paper and providing constructive comments. Many valuable suggestions have been made by Dr Riley, one of which led to the experiment for measuring tracer 'jitter' in the towing tank. The author would also like to extend his appreciation to Drs H.-P. Pao and C. E. Schemm, Applied Physics Laboratory, Johns Hopkins University, for their enthusiastic support throughout the project. In addition, the assistance of Messrs R. A. Srnsky and J. W. Waite in conducting the laboratory experiments and data analysis is appreciated. This work was sponsored by Navy Prime Contract No. N00024-81-C-5301, APL/JHU Subcontract No. 601395-S.

REFERENCES

BATCHELOR, G. K. 1959 Small-scale variation of convected quantities like temperature in turbulent fluid. Part 1. General discussion and the case of small conductivity. *J. Fluid Mech.* **5**, 113–133.

BENDAT, J. S. & PIERSOL, A. G. 1971 *Random Data Analysis and Measurement Procedures.* John Wiley.

BRITTER, R. E., HUNT, J. C. R., MARSH, G. L. & SNYDER, W. H. 1981 The effects of stable stratification on turbulent diffusion and the decay of grid turbulence. *J. Fluid Mech.* **127**, 27–44.

COMTE-BELLOT, G. & CORRSIN, S. 1966 The use of a contraction to improve the isotropy of grid-generated turbulence. *J. Fluid Mech.* **25**, 657–682.

COMTE-BELLOT, G. & CORRSIN, S. 1971 Simple Eulerian time correlation of full- and narrow-band velocity signals in grid-turbulence, 'isotropic' turbulence. *J. Fluid Mech.* **48**, 273–337.

DICKEY, T. D. & MELLOR, G. L. 1980 Decaying turbulence in neutral and stratified fluids. *J. Fluid Mech.* **99**, 13–31 (referred to herein as D&M).

FRIEHE, C. A. & SCHWARZ, W. H. 1970 Grid-generated turbulence in dilute polymer solutions. *J. Fluid Mech.* **44**, 173–193.

GAD-EL-HAK, M. 1972 Experiments on the nearly isotropic turbulence behind a jet grid. PhD dissertation, The Johns Hopkins University.

GREGG, M. C. 1980 Microstructure patches in the thermocline. *J. Phys. Oceanogr.* **10**, 915–943.

HINZE, J. O. 1959 *Turbulence.* McGraw-Hill.

HOLLIDAY, D. & MCINTYRE, M. E. 1981 On potential energy density in an incompressible, stratified fluid. *J. Fluid Mech.* **107**, 221–225.

ITSWEIRE, E. C., HELLAND, K. N. & VAN ATTA, C. W. 1986 The evolution of grid-generated turbulence in a stably stratified fluid. *J. Fluid Mech.* **162**, 299–338.

LANGE, R. E. 1974 Decay of turbulence in stratified salt water. PhD dissertation, University of California at San Diego.

LANGE, R. E. 1982 An experimental study of turbulence behind towed biplane grids in a salt-stratified fluid. *J. Phys. Oceanogr.* **12**, 1506–1513.

LIENHARD, J. H. & VAN ATTA, C. W. 1990 The decay of turbulence in thermally stratified flow. *J. Fluid Mech.* **210**, 57–112 (referred to herein as L&VA).

LIN, J.-T. & PAO, Y.-H. 1979 Wakes in stratified fluids. *Ann. Rev. Fluid Mech.* **11**, 317–338.

LIN, J.-T., PAO, Y.-H. & VEENHUIZEN, S. D. 1974 Turbulent wake of a propeller driven slender body in stratified and nonstratified fluids. *Bull. Am. Phys. Soc.* **19**, 1165.

LIN, J.-T. & VEENHUIZEN, S. D. 1974 Measurements of the decay of grid generated turbulence in a stably stratified fluid. *Bull. Am. Phys. Soc.* **19**, 1142–1143 (referred to herein as L&V).

LIU, H.-T. 1992 Effects of ambient turbulence on the decay of a trailing vortex wake. *J. Aircraft* **29**, 255–263.

LIU, H.-T. & LIN, J.-T. 1982 On the spectra of high-frequency wind waves. *J. Fluid Mech.* **123**, 165–185.

MÉTAIS, O. & HERRING, J. R. 1989 Numerical simulations of freely evolving turbulence in stably stratified fluids. *J. Fluid Mech.* **202**, 117–148.

MONIN, A. S. & YAGLOM, A. M. 1975 *Statistical Fluid Mechanics*, vol. 2, pp. 727–729. Massachusetts Institute of Technology Press.

ORSZAG, S. A. & PATTERSON, G. S. 1972 Numerical simulation of turbulence. In *Statistical Models and Turbulence*. Springer.

RILEY, J. J., METCALFE, R. W. & WEISSMAN, M. W. 1981 Direct numerical simulations of homogeneous turbulence in density-stratified fluids. In *Nonlinear Properties of Internal Waves, AIP Conf. Proc.*, vol. 76, pp. 79–112.

SCHEDVIN, J. A., STEGEN, G. R. & GIBSON, C. H. 1974 Universal similarity at high grid Reynolds numbers. *J. Fluid Mech.* **65**, 561–579.

STILLINGER, D. C. 1981 An experimental study of the transition of grid turbulence to internal waves in a salt-stratified water channel. PhD dissertation, University of California at San Diego.

STILLINGER, D. C., HELLAND, K. N. & VAN ATTA, C. W. 1983 Experiments on the transition of homogeneous turbulence to internal waves in a stratified fluid. *J. Fluid Mech.* **131**, 91–122.

VAN ATTA, C. W., HELLAND, K. N. & ITSWEIRE, E. C. 1984 The influence of stable stratification on spatially decaying vertically homogeneous turbulence. In *Proc. IUTAM Symp. on Turbulence and Chaotic Phenomena in Fluids, Sept. 1983*, Japan (ed. T. Tatsumi), p. 519. North Holland.

WILLIAMS, R. M. & PAULSON, C. A. 1977 Microscale temperature and velocity spectra in the atmospheric boundary layer. *J. Fluid Mech.* **83**, 547–567.

YOKOI, T. 1982 Observation of the lateral fluctuation of the laser beam passing through the atmosphere. *J. Geophys. Res.* **87**, 3149–3154.

YOON, K. & WARHAFT, Z. 1990 The evolution of grid-generated turbulence under conditions of stable thermal stratification. *J. Fluid Mech.* **215**, 601–638 (referred to herein as Y & W).